FINAL TECHNICAL REPORT

Award Number: 07HQGR0106

SOURCE PARAMETER STUDIES OF SOUTHEASTERN ALASKA EARTHQUAKES

Diane I. Doser
The University of Texas at El Paso
Department of Geological Sciences, 500 W. University Ave., El Paso, TX 79968
(915)-747-5851 (office), (915)-747-5073 (FAX), doser@utep.edu

ABSTRACT

This research focuses on the seismicity of southeastern Alaska from the Dixon Entrance to 61°N 139°W, a region in transition between the strike-slip faulting of the Queen Charlotte-southern Fairweather fault system and oblique convergent motion partitioned between strike-slip motion along the Denali and northern Fairweather fault systems and thrusting along faults of the St. Elias region. The tasks we proposed to accomplish in this study included: 1) Relocation of recent (1971-2005) background seismicity and examination of its relation to M>5 events and fault segmentation, 2) Examination of stress field variations from first motion analysis to determine how plate motion is partitioned within the region, 3) Comparison of the source processes of M>6.4 sequences along the Fairweather fault system through use of empirical Greens function analysis techniques, and 4) Study of intensity information to determine intensity decay with distance for comparison to other parts of Alaska.

INTRODUCTION

The southeastern Alaska area is a region in transition between the strike-slip motion of the Fairweather-Queen Charlotte fault system in the southern portion of region (Figure 1) and reverse-oblique motion of the Pacific and Yakutat blocks relative to North American west of ~ 140W. Total relative plate motion at Yakutat is estimated to be ~51 mm/yr in a direction of N15W (DeMets and Dixon, 1999) (Figure 1). Fletcher and Freymueller (2003) estimate that the northern Fairweather fault has a slip rate of ~44.6±2.0 mm/yr, one of the highest observed across any strike-slip fault in the world. The southern Denali fault system appears to be accommodating an additional 3.8±1.4 mm/yr of slip (Fletcher and Freymueller, 2003). Thus, a significant amount of convergence occurs across the northern Fairweather fault system, with Fletcher and Freymueller (1999) suggesting that much of the convergence could occur offshore, possibly along the Transition Fault zone (Figure 1).

In addition to tectonic deformation, significant glacier retreat in Glacier Bay and surrounding regions (Figure 1) has led to rapid uplift of the region (~ 17 mm/yr at Skagway, Larsen et al., 2003; over 30 mm/yr in portions of Glacier Bay and the Yakutat Icefields, Freymueller et al., 2008). Modeling of ice thinning by Sauber and Molnia (2004) in the Bering Glacier region to the west of the study area indicates that decreases in ice sheet thickness may hasten the occurrence of earthquakes with reverse/thrust mechanisms. A concentrated cluster of

earthquakes near Mt. Ogden southeast of Juneau (Figure 1) may also be related to hydrological or glacial changes (Wolf et al., 1997).

Southeastern Alaska has been the site of large (M>6.5) earthquakes along the Fairweather-Queen Charlotte fault system in 1927, 1949, 1972, 1958, and 2004 (Figure 2). Fletcher and Freymueller (2003) estimate that only 75 years is required to build up slip equivalent to the M_S=7.9 1958 earthquake along the northern Fairweather fault. Nishenko and Jacob (1990) have estimated a recurrence time of 120 to 130 years for earthquakes similar to the 1972 Sitka event and the 1949 M_S=8.1 Queen Charlotte earthquake located just south of the study area.

Previous studies (e.g. Horner, 1983; Horner et al., 1990; Perez and Jacob, 1980; Schell and Ruff, 1989; Doser and Lomas, 2000; Wolf et al., 1997; Doser, 2006), have either examined larger (M>5.0) earthquakes (relocations, limited source parameter studies), smaller magnitude events within localized regions (e.g. Glacier Bay, Mt. Ogden areas) or regional seismicity prior to the mid-1980's and thus do not provide a comprehensive view of regional background seismicity over the past ~35 years and how it may delineate barriers to rupture in larger events, stress changes, partitioning of plate motion, or identify other active faults.

In the following portion of this report we present new results from studies of phase, first motion and waveform information for southeastern Alaska. We focus on three separate regions: the southern Fairweather fault, the central Fairweather fault, and the northern Fairweather fault-Glacier Bay region

Earthquake Relocations

Doser and Lomas (2000) relocated larger (M>5.0) earthquakes occurring in the southeast region prior to 1971 using a master event technique. We have added to these results by relocating all earthquakes (regardless of magnitude) occurring within the region that had available phase data. Most phase data were taken from the listings of the International Seismological Summary (events prior to 1963) and the International Seismological Centre; however, we also used phase information from US Coast and Geodetic Survey circulars to relocate aftershocks of the 1958 Fairweather sequence. We used the jloc software package (Lee and Dodge, 2006) in the relocation process. This software uses a direct search routine specifically designed for locating poorly constrained earthquakes.

Earthquakes occurring between 1971 and 2005 were relocated using HypoDD (Waldhauser and Ellsworth, 2000). Phase data for these relocations were obtained from both the Alaska Earthquake Information Center (AEIC) and the Geological Survey of Canada (GSC) catalogs. Early in the study we found that the GSC catalog had a larger number of events than the AEIC catalog, especially for the northeastern portion of the study area. Thus we needed to merge the two catalogs while insuring we did not produce duplicates in the merged catalog.

Figures 3 and 4 show the results of the relocation process. Events occurring before 1972 (Figure 3) are primarily concentrated along the Fairweather fault system. There are moderate levels of seismicity in the Glacier Bay and Transition fault zone regions, as well as a few events located well east of the southern Fairweather system. Seismicity occurring since 1971 (Figure 4) shows an overall pattern similar to Figure 3, except that clusters of smaller magnitude events appear along the southern Fairweather fault, the southern Denali fault, and near Juneau.

We have divided the study area into three smaller regions for more detailed analysis of seismicity and its relationship to other geological and geophysical features. Figure 5 shows the seismicity of the southern Fairweather region. In this region earthquakes appear to be confined

to the Fairweather fault, with little recent seismicity occurring inboard of this feature. Virtually all the Fairweather fault in this region appears has ruptured within the past century (Figure 5a). The 1972 M_w=7.6 Sitka earthquake was a bilateral event with moment release along two large asperities (Schell and Ruff, 1989). The southern end of the rupture occurs near the intersection of the Fairweather and Chatham Strait faults. Rupture for the 1949 Queen Charlotte event (based on aftershock studies by Rogers, 1986) overlaps with a portion of the 1972 rupture. The 2004 Mw=6.8 earthquake appears to have ruptured a small asperity within the 1949 rupture zone, indicating there can be considerable variability in the rupture lengths of individual earthquakes along the Fairweather fault system. Aftershocks of the 2004 sequence occur near the northern edge of a portion of the Pacific plate that has been subducted beneath the northern Queen Charlotte Islands as delineated by Smith (1999) and Bustin (2006). Seismicity near -132° W in the southernmost part of the study area is related to reverse faults located on the eastern edge of Graham Island.

Figure 5b compares magnetic intensity data from Saltus et al. (1999) to seismicity and rupture segments along the Fairweather fault. The northern end of the 1949 rupture occurs near a change in the pattern of magnetic anomalies within the Pacific plate. The southeastern end of the 1972 rupture and northwestern end of the 2004 rupture appear to occur at the edge of a magnetic high within the Pacific plate.

The seismicity of the central Fairweather region is shown in Figure 6. This includes the northern portion of the 1972 rupture zone, the southern portion of the 1958 rupture zone, and the 1927 rupture zone, all along the Fairweather fault. Most earthquakes located along the Fairweather fault are larger magnitude aftershocks of these historic sequences. The intersection of the Transition and Fairweather faults appears to have served as a barrier to rupture in 1927 and 1972. Although strike-slip motion dominates along the Fairweather fault, the presence of Mt. Edgecumbe (triangle, Figure 6a) a volcano with Holocene age lava flows (Brew, 1994) near Sitka, indicates some localized pull-apart extension may be occurring.

The lack of recent seismicity along the fault zone could be real, or could be related to the fact that seismograph station coverage within the region is poor (Figure 1). Smaller magnitude, recent earthquakes are associated with the Transition fault zone; site of the 1973 Cross Sound sequence, and the Spencer Passage region

The Transition fault zone marks the southern end of the Yakutat block. North of the Transition fault zone/Fairweather fault zone intersection the Fairweather fault begins to bend toward the northwest. The role the Transition fault zone plays in active deformation of the region is highly debated. First motion (Perez and Jacob, 1980) and waveform modeling (Doser and Lomas, 2000) studies of the 1973 Cross Sound sequence indicate that thrust faulting is occurring at least along the southern end of the Transition fault system. Relocations of earthquakes of the 1899 Yakutat sequence (Doser, 2006) also suggest that at least one event of this sequence is likely associated with the Transition fault zone. Seismic reflection data suggest that some portions of the Transition fault zone may not have been active since the Miocene (Bruns, 1985). However GPS data and other tectonic modeling (e.g. Fletcher and Freymueller, 1999; Pavlis et al., 2004) suggest that the Transition fault zone could accommodate up to 20 mm/yr of convergence.

Figure 6b compares magnetic intensity data to seismicity. A large negative anomaly is associated with Mt. Edgecumbe. The 1973 Cross Sound events appear to have occurred within a magnetic high located north of the Transition fault zone. There does not appear to be a relation

between the magnetic anomalies along the central Fairweather fault system and fault segmentation during large earthquakes along the system.

The northern Fairweather fault system (Figure 7) is the most seismically active portion of our study area. Seismicity is associated with the entire northern trace of the fault which ruptured in 1958 (Figure 7a). The seismicity intensifies along the fault at the western end of the study area, but there is an apparent gap in the seismicity in the region where the Fairweather and Boundary faults intersect. There are clusters of activity north of Glacier Bay, east (Mt. Ogden) and north of Juneau, and at the intersection of the Denali and Gastineau Channel fault.

Magnetic intensity data (Figure 7b) are sparse for the region north of Glacier Bay (59 to 60°N, 134 to 138°W). There appears to be little correlation between the magnetic anomalies and seismicity.

We compare uplifted regions (Freymueller et al., 2008) to seismicity in Figure 7c. Shaded regions have uplifts > 30 mm/yr. Note that the most quiescent portion of the Fairweather fault is associated with a region of very high uplift in the Yakutat ice fields, while clusters of seismicity occur near its edges. Small areas of uplift in western Glacier Bay and northeastern Chatham Strait also appear relatively quiescent; however the region of highest uplift in northern Glacier Bay is located in an area of intense seismicity. The uplift in the Glacier Bay region is in response to deglaciation over the past ~250 years, while the uplift in the Yakutat ice fields is related to ice loss over the past 100 years (Freymueller et al., 2008). Thus not only the amount but the duration of uplift due to deglaciation may influence seismicity within this region.

Stress Inversions

Few estimates of the orientation of stress have been made in southeastern Alaska. Ristau et al. (2007) used moment tensors and first motion focal mechanisms of moderate sized earthquakes to determine the orientation of stress for the eastern Yakutat region (57° to 61°N, 135° to 140°W) and the northern Queen Charlotte fault (53.5° to 55.5°N). Their results (Figure 8a, Table 1) show near horizontal, north-northeast directed maximum compressive stress (σ_1) in both regions. Minimum compressive stress (σ_3) is oriented east-southeast but changes from near horizontal in the south to steeply plunging (52°) in the north, indicating increasing convergence along the northern Fairweather fault system. Ruppert (2008) used earthquake focal mechanisms to determine the stress orientation of the region located between the Fairweather and Denali faults from northern Glacier Bay to western Yakutat Bay. Her results (Figure 8a, Table 1) indicate southeast striking, near horizontal σ_1 with a northwest striking, steeply plunging (64°) σ_3.

We attempted to directly invert first motion data from clusters of recent earthquakes to determine stress orientations using the technique of Robinson (1999). Many regions did not have a sufficient number of events or first motion observations for analysis; however results for four regions are shown in Figures 8a and 8b, as well as Table 1. These results were obtained by 1000 repeated inversions of the randomly perturbed first motion data.

Inversion of first motion data for the northern Glacier Bay region gave a northwest oriented, near horizontal σ_1 direction with σ_3 striking WSWand plunging 70°. This stress orientation favors faulting along ENE-WSW oriented reverse faults. An Mw 6.0 earthquake occurring in this region in 1952 showed a northwest oriented slip vector, but with a larger component of strike-slip motion (Doser and Lomas, 2000).

We were able to obtain stress orientations for events associated with two segments of the northern Fairweather fault. The first region (NF1) extends from the intersection of the

Fairweather and Peril Strait faults to Dry Bay (Figure 8a). The second region (NF2) includes events located just east of Yakutat Bay. The NF1 region shows σ_1 striking 70° with a horizontal plunge and σ_3 plunges vertically. This would favor reverse faulting on NNW-SSE oriented faults. Region (NF2) gave a stress orientation (Table 1) favorable for movement on north-south oriented reverse faults.

A sufficient number of first motions were not available for stress determination in the Mt. Ogden region; however the available data (Figure 8b) suggest reverse oblique faulting may be occurring. Seismicity in the region is observed to trend northeast-southwest with a high angle of dip to the northwest; a fault orientation consistent with the first motion data (Figure 8b) and suggesting reverse-oblique motion. The orientations of the P- and T-axes for this mechanism are shown in Figure 8a (dashed lines).

The stress orientation information (Figure 8a) indicates that along much of the Fairweather fault system seismicity is presently responding to a northeast oriented σ_1, although slip-vectors for large strike-slip events along the system are oriented in the direction of plate motion (Doser and Lomas, 2000). Thus moderate magnitude background seismicity is responding to the component of convergence between the Pacific and North American plates. Inboard of the Fairweather fault system, at least in portions of the Glacier Bay and Mt. Ogden regions, σ_1 is more closely aligned to the direction of plate motion. GPS data presented by Freymueller et al. (2008) and Mazzotti et al. (2008) show velocity vectors at sites near the Fairweather fault that are oriented in the direction of plate motion, with rotation of velocity vectors to the northeast along the Denali fault and oriented near north-south in the central Glacier Bay region. Northwest directed velocity vectors observed in the region near Mt. Ogden (Mazzotti et al., 2008) are consistent with the P-axes orientation determined for the Mt. Ogden sequence (Figure 8a). These results indicate that moderate seismicity, especially in the northern study area extending from Cross Sound to Yakutat Bay, could occur along reverse faults with a variety of azimuths. This is consistent with both the historical seismicity (Doser and Lomas, 2000) and recent moment tensor solutions (Ristau et al., 2007).

Source Processes/Empirical Greens Function Evaluations

We have determined the source processes of moderate to large magnitude earthquakes along the Fairweather fault system using an empirical Greens function (EGF) technique where a smaller event with a location and focal mechanism similar to a large event of interest (both recorded at the same station) is treated as a Greens function (representing the path effects between the source region and a station) and is deconvolved from the larger event. The result of the deconvolution provides information on the larger event's rupture history/rupture complexity (e.g. rupture directivity, variation of moment release) as well as stress drop estimates.

Figure 9 shows a map of the EGF pairs that we have used in our analysis (see Table 2 for more details on the event pairs). The first pair occurred north of Glacier Bay and the second near Lituya Bay along the Fairweather fault. Pairs 3 and 4 are part of the 1973 Cross Sound sequence. Pair 5 is part of the 2004 M_w=6.8 southern Fairweather fault sequence, pair 7 occurs along the southern Queen Charlotte fault system and pair 6 occurred to the east. Digital seismograms from Canadian and Alaskan broadband stations were used in the analysis, except for the 1973 sequence where we digitized scanned seismograms from Worldwide Standardized Seismological Network (WWSSN) stations.

We demonstrate our analysis process in Figures 10 through 12. Figure 10 shows the P-wave arrivals recorded at seismograph station BESE (Bessie Mountain, triangle, Figure 9) for the

2004 Fairweather mainshock (top) and smaller aftershock (bottom) that was used as the EGF. Frequency spectra of the two windowed P-arrivals and the quotient of the spectra are shown in Figure 11. The spectral quotient represents the relative source-time function (RSTF) of the mainshock in the frequency domain. In order to stabilize the spectral quotient prior to transformation back to the time domain we bandpass filter the quotient and use the fraction parameter water level technique (Helmberger and Wiggins, 1971; Mueller, 1985) to reduce the effect of zeroes in the denominator of the quotient. We then transform the quotient to the time domain to obtain our RSTF (Figure 12). In this case the rupture appears to be simple with a duration of ~10 seconds.

When more than one station has recorded an event pair, we combine RSTF's from all stations to determine a stacked and average RSTF. Figure 13 illustrates this process for the 2004 mainshock located north of Glacier Bay. Note that the RSTF shape appears simple at all stations, although at station PIN, located to the west-northwest of the event (Figure 9), the RSTF is considerably broader. Since one nodal plane of the AEIC moment tensor for this event strikes 280°, this may suggest rupture along this plane toward the east-southeast, which would cause broadening of the RSTF at station PIN. Next we estimate the seismically radiated energy in the time domain by determining the area beneath the averaged and stacked RSTF's. We also can estimate the radiated energy by integrating the average and stacked RSTF's in the frequency domain. Finally, we use the seismically radiated energy to estimate Orowan's (1960) stress drop.

Figure 14 shows estimates of stress drop for the 7 events based on the 4 different methods of calculating seismically radiated energy. Squares represent events on the Fairweather-Queen Charlotte fault system, triangles events of the 1973 Cross Sound sequence, and diamonds events that occurred off of major fault systems. Note the highest stress drops are associated with the 1973 Cross Sound sequence (occurring on reverse faults possibly associated with the Transition fault zone). The stress drop estimates for event 6, occurring southeast of the Queen Charlotte Islands (Figure 9) are also high. Stress drops for events 5 and 7, which likely occurred on the Queen Charlotte-Fairweather fault system, are low for their respective moments, suggesting lower stress drops may be associated with events occurring along well established fault zones. The stress drop estimates for event 2, a reverse-oblique event near the Fairweather fault, are also lower than those for event 1, a reverse-oblique event located north of Glacier Bay.

Faulting Processes of the 1958 Fairweather Earthquake

We have re-examined the waveforms of the 1958 M_S 7.9 Fairweather earthquake in an effort to better determine its rupture history and its relation to geologic and geophysical features along the fault. In addition, we have relocated all recorded aftershocks for a one month period following the mainshock and all possible foreshocks occurring within three months of the mainshock.

The jloc algorithm was used for all relocations (Figure 15). The closest events occurring prior to the mainshock (orange stars, Figure 15) are located well to the west of the mainshock and thus do not appear to be foreshocks. Aftershocks (plusses, Figure 15) occur over a 400 km long zone extending from the intersection of the Transition fault zone with the Fairweather fault northwest to the Pamplona fault zone. The arrows indicate the maximum estimated extent of the aftershock zone. The error ellipses for most locations are elongated in a northeast-southwest direction as indicated by the ellipse associated with the event on June 19. This elongation is due to seismograph station coverage during this period of time. The aftershock symbols are color

coded based on the length of their error ellipses, with red symbols having maximum ellipse axes < 85 km in length. Note that many of the aftershocks concentrate in the region between the Fairweather fault and the Transition fault zone. The triangle represents the intensity center for the mainshock (Doser, 2009).

We re-analyzed the highest quality P-waveforms from the mainshock in order to better relate moment release during the mainshock with the aftershock pattern and known changes in geology/geophysics along the rupture zone. Our new results (Figure 16) give a much longer and more complicated rupture history than the initial studies of Doser and Lomas (2000). The new source time function shows 4 peaks in moment release with a total duration of 74 sec. Assuming unilateral rupture (based on the position of the mainshock epicenter relative to the observed surface faulting) with a velocity of 3.5 km/sec gives a total rupture length of ~ 260 km. We obtain a total moment release of 4.8 x 10^{20} N-m, equivalent to an M_w 7.8 These estimates are closer to rupture length and moment estimates based on surface wave modeling (Ben-Menahem and Toksoz, 1963) and the average fault slip of 3.5 m is comparable to that observed by Plafker et al. (1978) at the surface.

Figure 17 shows our interpretation of rupture history based on the duration and amplitude of the source-time function. The estimated seismic slip in meters on each segment is given in italics. Surface measurements of slip from Plafker et al. (1978) are indicated by boxes and bold red numbers. The first peak in moment release corresponds to rupture between the hypocenter and Mt. Fairweather (denoted by X labeled MF) where there is a bend in the fault trace. This is followed by a second peak in moment release along the fault between Mt. Fairweather and Lituya Bay (LB, Figure 17). This peak in moment release (the highest during the event, Figure 16) may have been responsible for triggering the giant landslide and resulting tsunami within Lituya Bay. The next peak in moment release occurred near Dry Bay (DB, Figure 17) where the Fairweather and Boundary faults intersect. This peak may be responsible for the severe intensities observed in the Dry Bay region, resulting in the location of the event's intensity center within this region. This high moment release also occurs on the segment of the fault that crosses the Yakutat ice fields where maximum uplift has been observed by Freymueller et al. (2008) (Figure 7c). A final peak in moment release appears to have occurred near the end of the fault rupture at the point the Fairweather fault changes strike at the eastern edge of Yakutat Bay. Limited gravity data for the region (Saltus et al., 2008) (Figure 18) show a Bouguer anomaly high along the fault zone in the region of maximum moment release between Mt. Fairweather and Lituya Bay. A smaller high occurs in the region northeast of Dry Bay. These anomaly highs may indicate changes in bedrock geology that could control the location of asperities along the fault.

Figure 19 compares moment release (bottom) and slip (top) for the 1958 Fairweather and 2002 Denali fault earthquakes. Both have comparable surface wave magnitudes and involved predominantly unilateral rupture along strike-slip faults. The Denali fault moment release was obtained from Ozacar and Beck, (2004) and the surface slip data from Eberhardt-Phillips et al. (2003). It appears the 2002 event had a much higher peak in moment release (gray region) than the 1958 event, in addition to the moment released as the event initiated along the Susitna Glacier thrust (striped region) . Plafker et al. (1978) were only able to collect limited slip measurements along the 1958 Fairweather fault rupture zone due to the difficulty in finding exposures of the fault in rugged, ice covered terrain (dashed lines). These slip values appear to underestimate the total slip from seismic information (solid lines), which is more comparable to

surface offsets measured along the Denali fault (plusses). These results suggest that the 2002 and 1958 events were indeed comparable in size.

Finally, we have used the GNStress_2 software package developed by Robinson (2005) to examine the change in Coulomb failure stress (ΔCFS) following the 1958 mainshock assuming a regional background stress orientation similar to that determined by Ruppert (2008). Although we tested a wide variety of possible focal mechanism orientations for ΔCFS following the 1958 mainshock (including focal mechanisms similar to the mainshock, the 1973 Cross Sound events, and the 1979 St. Elias event to the northwest), we found that faulting along east-west oriented reverse faults (strike=260, dip=50, rake=110) gave the highest percentage (76%) of aftershocks located within regions of positive ΔCFS (Figure 20).

Intensity Studies

We have developed intensity attenuation relationships for southeastern Alaska as part of a larger study of Alaskan intensity information. We then used the relationship to estimate magnitudes and locations of historic (pre-1960's) seismicity in southeastern Alaska. Figure 21 shows the calibration events we used to develop the attenuation relationship for the southeast region, an area that extends as far west as the Pamplona fault zone. The attenuation relationship predicts observed intensities for two calibration events well (Figure 22), in spite of the sparse regional population distribution that leads to limited intensity observations. Figure 23 shows results of the analysis of historic events using the intensity attenuation relationship. It appears that the September 4, 1899 (M_S 7.9) earthquake is likely associated with the Pamplona fault zone (Figure 23a), while the September 10 events (Figure 23b and 23c) occurred near Yakutat Bay. An event in 1907 (with a newly estimated intensity magnitude of 6.0) could have occurred anywhere between the Denali and Fairweather faults (Figure 23d), while a M_S 7.0 event in 1908 likely occurred offshore between the Pamplona fault zone and Yakutat Bay (Figure 23e), possibly along the Transition fault zone. The November 12, 1927 event appears to be an aftershock of the 1927 Sitka sequence (with newly estimated intensity magnitude of 6.0) (Figure 23f). Finally, the intensity center for the 1958 Fairweather earthquake is located near Dry Bay (Figure 23g). Complete results of this study can be found in Doser (2009).

Related Studies

Results of previously funded NEHRP research on seismicity of the Prince William Sound, Alaska region was published in a American Geophysical Union Monograph on "Active Tectonics and Seismic Potential of Alaska" (Doser et al., 2008). A paper on seismicity of the entire plate boundary region between 59° and 62° N and 146° and 154° W is in press for the August 2009 edition of the *Bulletin of the Seismological Society of America.*

We are continuing work on a study of recent and historic seismicity of interior Alaska. We hope to complete a draft of our work related to the region located between the Kobuk and Kaltag-Tintina fault systems by December 2009.

We have recently begun a NEHRP funded study of seismicity occurring between the Fairweather-Chugach St. Elias fault system and the Denali fault system, located north and west of the study area we focused on in this report. We hope to better determine the linkages between these fault systems, as well as examining variations in the source processes of earthquakes within this region.

.

Reports Published

Doser, D.I., Estimating magnitude and location of Alaskan earthquakes using intensity data, in press, Bull. Seismol. Soc Amer., July 2009.

Doser, D.I., The Rupture Processes of the 1958 Fairweather Fault, Alaska, Earthquake Sequence, Fall Meeting, American Geophysical Union, Abstract S23B-1898, 2008.

Doser, D.I., Estimating magnitude and location from intensity for three regions of Alaska, Seismol. Res. Lett. 79, 322, 2008.

Escudero, C.S., and D.I. Doser, Relative source time function studies of earthquakes in southeastern Alaska, Fall Meeting, American Geophysical Union, Abstract S23B-1894, 2008.

Escudero, C.S., and D.I. Doser, Relative source time function studies of earthquakes in southeastern Alaska, Seismol. Res. Lett. 79, 350, 2008.

Rodriguez, H. and D. Doser, Earthquake relocation studies in southeastern Alaska, Seismol. Res. Lett. 79, 294, 2008.

Rodriguez, H. and D. Doser, Background seismicity study of Southeastern Alaska, Fall Meeting, American Geophysical Union, Abstract S23B-1895, 2008.

Availability of Data Sets

Copies of phase data for earthquakes and digital/digitized seismograms used in this study may be obtained from Dr. Diane Doser, (915)-747-5851 or doser@ utep.edu.

Bibliography

Ben-Menahem, A., and M.N. Toksoz, Source-mechanism from spectra of long-period seismic surface wave, 3. The Alaska earthquake of July 10, 1958, Bull. Seismol. Soc. Am. 53, 905-919, 1963.

Brew, D.A., Latest Mesozoic and Cenozoic magmatism in southeastern Alaska, in: Plafker, G. and H.C. Berg (eds.), The Geology of Alaska, The Geology of North America Vol. G-1, Geol. Soc. Amer., 621-656, 1994.

Bruns, T.R., Tectonics of the Yakutat block, an allochthonous terrane in the northern Gulf of Alaska, U.S. Geol. Surv. Open File Rept. 85-13, 112 pp., 1985.

Bustin, A.M.M., The crustal structure, deformation from GPS, and seismicity related to oblique convergene along the Queen Charlotte margin, British Columbia, Ph.D. dissertation, University of Victoria, British Columbia, 226 pp., 2006.

DeMets, C., and T.H. Dixon, New kinematic models for Pacific-North America motions from 3 Ma to present, 1: Evidence for steady motion and biases in the NUVEL-1A model, Geophys. Res. Lett. 26, 1921-1924, 1999.

Doser, D.I., Estimating magnitude and location of Alaskan earthquakes using intensity data, in press, Bull. Seismol. Soc Amer., July 2009.

Doser, D.I., Relocation of earthquakes (1899-1917) in south-central Alaska, Pure and Appl. Geophys., 163, 1461-1476, 2006.

Doser, D. I., and Lomas, R., The transition from strike-slip to oblique subduction in southeastern Alaska from seismological studies, Tectonophysics 316, 45-65, 2000.

Eberhart-Phillips, D. P. J. Haeussler, J. T. Freymueller, A. D. Frankel, C. M. Rubin, P. Craw, N. A. Ratchkovski, G. Anderson, G. A. Carver, A. J. Crone, T. E. Dawson, H. Fletcher, R. Hansen, E. L. Harp, R. A. Harris, D. P. Hill, S. Hreinsdóttir, R. W. Jibson, L. M. Jones, R. Kayen, D. K. Keefer, C. F. Larsen, S. C. Moran, S. F. Personius, G. Plafker, B. Sherrod, K. Sieh, N. Sitar, and W. K. Wallace, The 2002 Denali fault earthquake, Alaska: a large magnitude, slip partitioned event, Science 300, 1113–1118, 2003.

Fletcher, H.J., and J. T. Freymueller, New constraints on the motion of the Fairweather

fault, Alaska, from GPS observations, Geophys. Res. Lett. 30, 1139, doi:10.1029/2002GL016476, 2003.

Fletcher, H.J., and J.T. Freymueller, New GPS constraints on the motion of the Yakutat block, Geophys. Res. Lett. 26, 3029-3032, 1999.

Freymueller, J.T., H. Woodard, S.C. Cohen, R. Cross, J. Elliott, C.F. Larsen, S.Hreinsdóttir, and C. Zweck, Active deformation processes in Alaska, based on 15 years of GPS measurements, in American Geophysical Union Monograph 179 on "Active Tectonics and Seismic Potential of Alaska", J. T. Freymueller, P.J. Hauessler, R. Wesson and G. Ekstrom (eds.), 1-42, 2008.

Helmberger, D., and Wiggins, R.A., Upper mantle structure of midwestern United States, J. Geophys. Res. 76, 3229-3244, 1971.

Horner, R.B., Seismicity in the St. Elias region of northwestern Canada and southeastern Alaska, Bull. Seism. Soc. Am. 73, 1117-1137, 1983.

Horner, R.B., Seismicity in the Glacier Bay region of southeast Alaska and adjacent areas of British Columbia, in: Milner, A.M. and J.D. Wood, Jr., Eds., Proc. 2nd Glacier Bay Sci. Symp. Glacier Bay Lodge, Alaska, Sept. 1988, 6-11, 1990.

Larsen, C.F., K.A. Echelmeyer, J.T. Freymueller, and R.J. Motyka, Tide gauge records of uplift along the northern Pacific-North American plate boundary, 1937 to 2001, 2003.

Lee, W.H.K., and D.A. Dodge, Development of a direct search software package for locating poorly constrained earthquakes, Seismol. Res. Lett. 77, 292, 2006.

Mazzotti, S., L. Leonard, R.D. Hyndman, and J.F. Cassidy, Tectonics, dynamics and seismic hazard in the Canada-Alaska cordillera, in American Geophysical Union Monograph 179 on "Active Tectonics and Seismic Potential of Alaska", J. T. Freymueller, P.J. Hauessler, R. Wesson and G. Ekstrom (eds.), 297-320, 2008.

Mueller, C. S., Source pulse enhancement by the deconvolution of an empirical Green's function. Geophysical Research Letters 12, 33-36, 1985.

Nishenko, S.P., and K.H. Jacob, Seismic potential of the Queen Charlotte-Alaska-Aleutian-seismic zone, J. Geophys. Res. 95, 2511-2532, 1990.

Orowan, E., Mechanism of faulting, Chapter 12, D.T. Griggs (ed.), Geol. Soc. Am Mem 79, 323-345, 1960.

Ozacar, A.A., and S.L. Beck, The 2002 Denali fault and 2001 Kunlun fault earthquakes; complex rupture processes of two large strike-slip events, Bull. Seismol. Soc. Am. 94 B, 278-292, 2004.

Pavlis, T.L., C. Picornell, L. Serpa, R. Bruhn, and G. Plafker, Tectonic processes during oblique collision: insights from the St. Elias orogen, northern North America Cordillera, Tectonics 23, doi:10.1029/2003TC001557, 2004.

Perez, O., and K.H. Jacob, Tectonic model and seismic potential of the eastern Gulf of Alaska and Yakataga seismic gap, J. Geophys. Res. 85, 7131-7150, 1980.

Plafker, G., T. Hudson, T.R. Bruns, and M. Rubin, Late Quaternary offsets along the Fairweather fault and crustal plate interactions in southern Alaska, Can. J. Earth Sci. 15, 805-816, 1978.

Plafker, G., L.M. Gilpin, and J. C. Lahr, Neotectonic map of Alaska, in The Geology of North America, vol. G-1, The geology of Alaska (G. Plafker and H.C. Berg, eds.), Geol. Soc. Amer., Boulder, Colo., pp. 389-449, 1994.

Ristau, J., G.C. Rogers, and J.F. Cassidy, Stress in western Canada from regional moment tensor analysis, Can. J. Earth Sci. 44, 127-148, 2007.

Robinson, R., GNStress2: A computer programme for calculating the induced stress in a region due to slip on one or more faults, 12 pp. (copy of software available at ftp.gns.cri.nz), 2005.

Robinson, R., Get Stress: A Computer Programme for Inverting First Motion Observations to a Regional Stress Tensor, Institute of Geological and Nuclear Sciences, Lower

Hutt, New Zealand, 7 pp. (copy of software available at ftp.gns.cri.nz/pub/robinson/getstress), 1999.

Rogers, G.C., Seismic gaps along the Queen Charlotte Fault, Earthq. Predit. Res., 4, 1-11, 1986.

Ruppert, N.A., Stress map for Alaska from earthquake focal mechanisms, in American Geophysical Union Monograph 179 on "Active Tectonics and Seismic Potential of Alaska", J. T. Freymueller, P.J. Hauessler, R. Wesson and G. Ekstrom (eds.), 351-368, 2008.

Saltus, R.W., P.J. Brown II, R.L. Morin, and P.L. Hill, 2006 Compilation of Alaska Gravity Data and Historical Reports, U.S. Geol. Surv. Data Series Report 264, 2008.

Saltus, R.W., G.G. Connard and P.L. Hill, Alaska Aeromagnetic Compilation-Digital Grids and Survey Data, U.S. Geol. Surv. Open File Rept. 99-502, 1999.

Sauber, J. M., and B. Molnia, Glacial ice mass fluctuation and fault instability in tectonically active southern Alaska, Global and Planet. Change 42, 279-293, 2004.

Schell, M.M., and L.J. Ruff, Rupture of a seismic gap in southeastern Alaska: the 1972 Sitka earthquake (Ms 7.6), Phys. Earth Planet. Int. 54, 241-257, 1989.

Smith, R.A.J., Structure, deformation, and thermal regime of the Queen Charlotte Transform margin: MS thesis, University of Victoria, British Columbia, 179 pp., 1999.

Waldhauser, F., and W.L. Ellsworth, A double-difference earthquake location algorithm: method and application to the northern Hayward fault, California, Bull. Seismol. Soc. Am. 90, 1353-1368, 2000.

Wolf, L.W., C.A. Rowe and R.B. Horner, Periodic seismicity near Mt. Ogden on the Alaska-British Columbia border: a case for hydrologically triggered earthquakes?, Bull. Seism. Soc. Am. 87, 1473-1483, 1997.

Table 1 – Stress Analysis Information

Region	Number events	σ_1 (strike, plunge)	σ_3 (strike, plunge)	Reference
Eastern Yakutat	19	26, 5	122, 52	Ristau et al. (2007)
Northern Queen Charlotte Fault	18	27, 10	177, 1	Ristau et al. (2007)
Between Denali and Fairweather faults	12	216, 10	328, 64	Ruppert (2008)
Glacier Bay (GB)	133	340, 0	250, 70	This study
North Fairweather 1 (NF1)	206	70, 0	70, 90	This study
North Fairweather 2 (NF2)	158	300, 10	150, 80	This study
Mt. Ogden	170	345, 1 (P-axis)	76, 28 (T-axis)	This study

Table 2 – Event Pairs Used for Empirical Greens Function Studies

Event Pair	Date	Time	Magnitude	Latitude	Longitude
1	8/4/2004 4/8/2005	0113 0938	5.1 Mw 3.6 Mw	59.38 59.35	-136.32 -136.45
2	8/3/2008 7/1/2008	0944 0253	4.5 ML 2.7 ML	58.72 58.77	-137.38 -137.49
3	7/1/1973 7/3/1973	1333 1659	6.7 Mw 6.1 Mw	57.86 57.99	-137.42 -138.04
4	7/3/1973 7/5/1973	1659 0749	6.1 Mw 5.4 Mw	57.99 57.9	-138.04 -137.99
5	6/28/2004 7/4/2004	0949 2317	5.9 Mw 4.5 Mw	54.80 55.04	-134.24 -134.58
6	6/20/2006 8/8/2008	1002 1541	5.3 Mw 4.1 Mw	52.22 51.90	-131.02 -131.24
7	1/9/2008 8/8/2008	1440 1541	5.9 Mw 4.1 Mw	51.69 51.90	-131.13 -131.24

Table 3 – Estimated Moments and Stress Drops from Empirical Greens Function Studies

Event	Moment (N-m)	$\Delta\sigma_1^*$ Pa	$\Delta\sigma_2^*$ Pa	$\Delta\sigma_2^*$ Pa	$\Delta\sigma_4^*$ Pa
1	$1.4\text{x}10^{20}$	$7.1\text{x}10^{4}$	$1.2\text{x}10^{6}$	$5.7\text{x}10^{6}$	$9.2\text{x}10^{7}$
2	$4.2\text{x}10^{19}$	1.2	29	470	$1.2\text{x}10^{4}$
3	$1.4\text{x}10^{23}$	$1.4\text{x}10^{10}$	$2.2\text{x}10^{11}$	$2.3\text{x}10^{15}$	$3.6\text{x}10^{16}$
4	$1.8\text{x}10^{22}$	$1.3\text{x}10^{9}$	$1.2\text{x}10^{10}$	$2.6\text{x}10^{14}$	$2.4\text{x}10^{15}$
5	$1.9\text{x}10^{23}$	$5.9\text{x}10^{5}$	$1.5\text{x}10^{7}$	$1.9\text{x}10^{8}$	$4.8\text{x}10^{9}$

6	$2.7x10^{19}$	$9.1x10^{7}$	$8.2x10^{8}$	$3.1x10^{10}$	$2.8x10^{11}$
7	$8.8x10^{21}$	$1.9x10^{4}$	$1.7x10^{5}$	$5.6x10^{6}$	$5.1x10^{7}$

* $\Delta\sigma_1$ estimate from area under average RSTF measured in time domain, $\Delta\sigma_2$estimate from area under stacked RSTF measured in time domain, $\Delta\sigma_3$ estimate from average RSTF measured in frequency domain, $\Delta\sigma_4$ estimate from stacked RSTF measured in frequency domain.

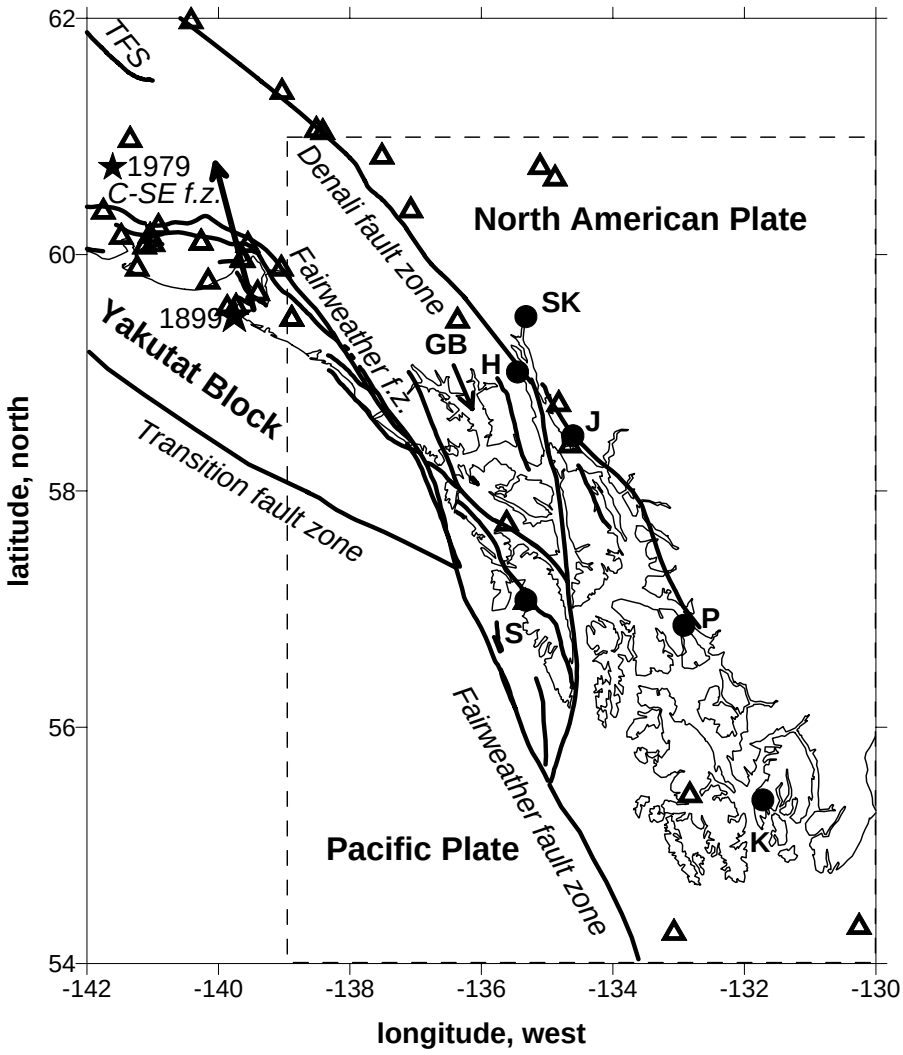

Figure 1 – Southeastern Alaska study area (dashed box). Stars are M > 7.0 earthquakes occurring outside study area. Arrow shows motion of Yakutat block relative stable North America (DeMets and Dixon, 1999). C-SE f.z. is the Chugach-St. Elias fault zone, TF is Totschunda fault system. Triangles are seismograph station locations. Cities are denoted by dots. GB is Glacier Bay. H=Haines, J=Juneau, K=Ketchikan, P=Petersburg, S=Sitka, SK=Skagway. Quaternary faults are from Plafker et al. (1994).

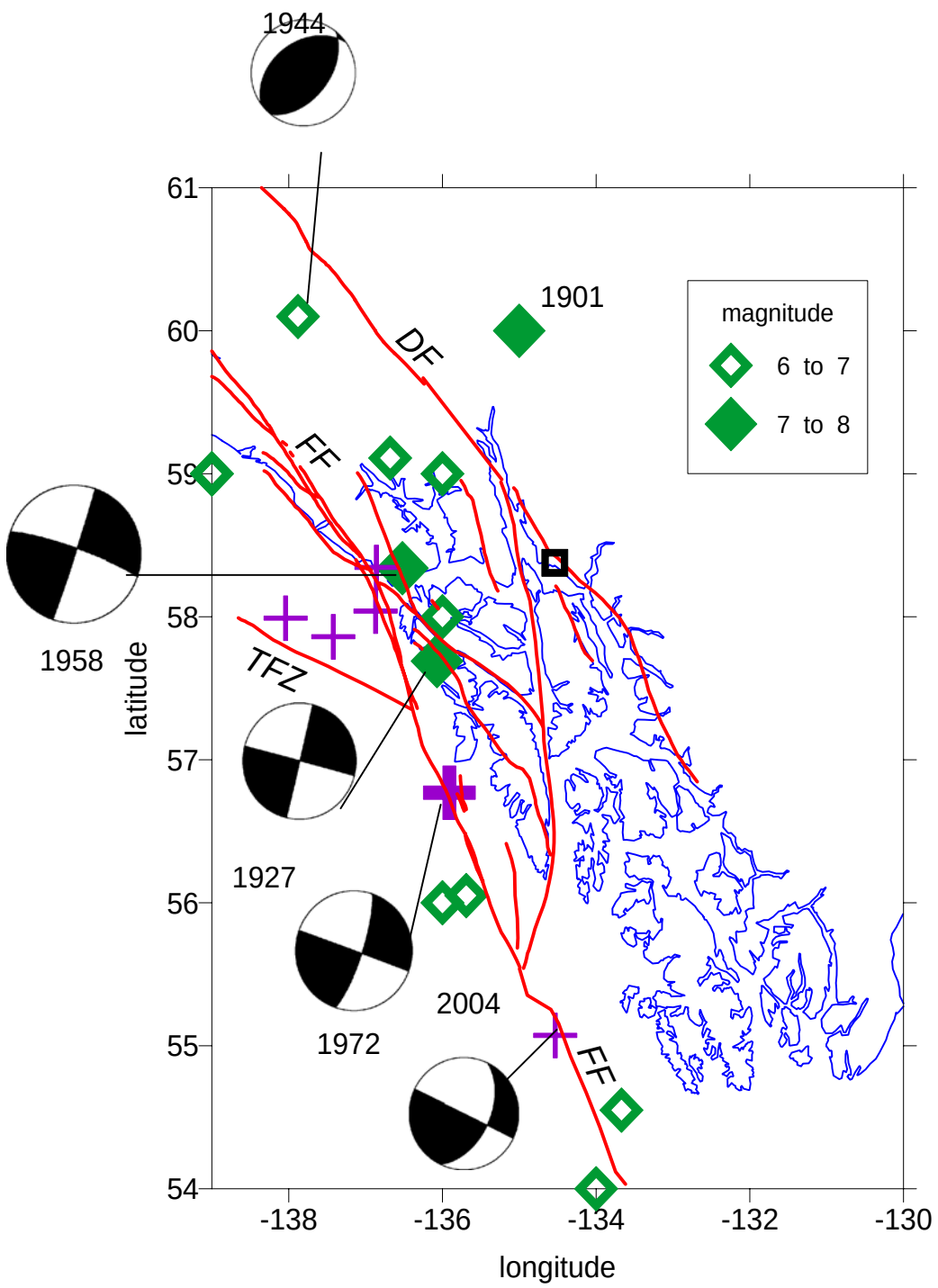

Figure 2 - Magnitude ≥ 6.0 earthquakes of study area. Diamonds are earthquakes occurring prior to 1971. Focal mechanisms are from Doser and Lomas (2000), except for 2004 event which is a Canadian moment tensor solution (J. Cassidy, pers. com.., 2006). DF=Denali fault, FF= Fairweather fault, TFZ=Transition zone fault. Box is Juneau

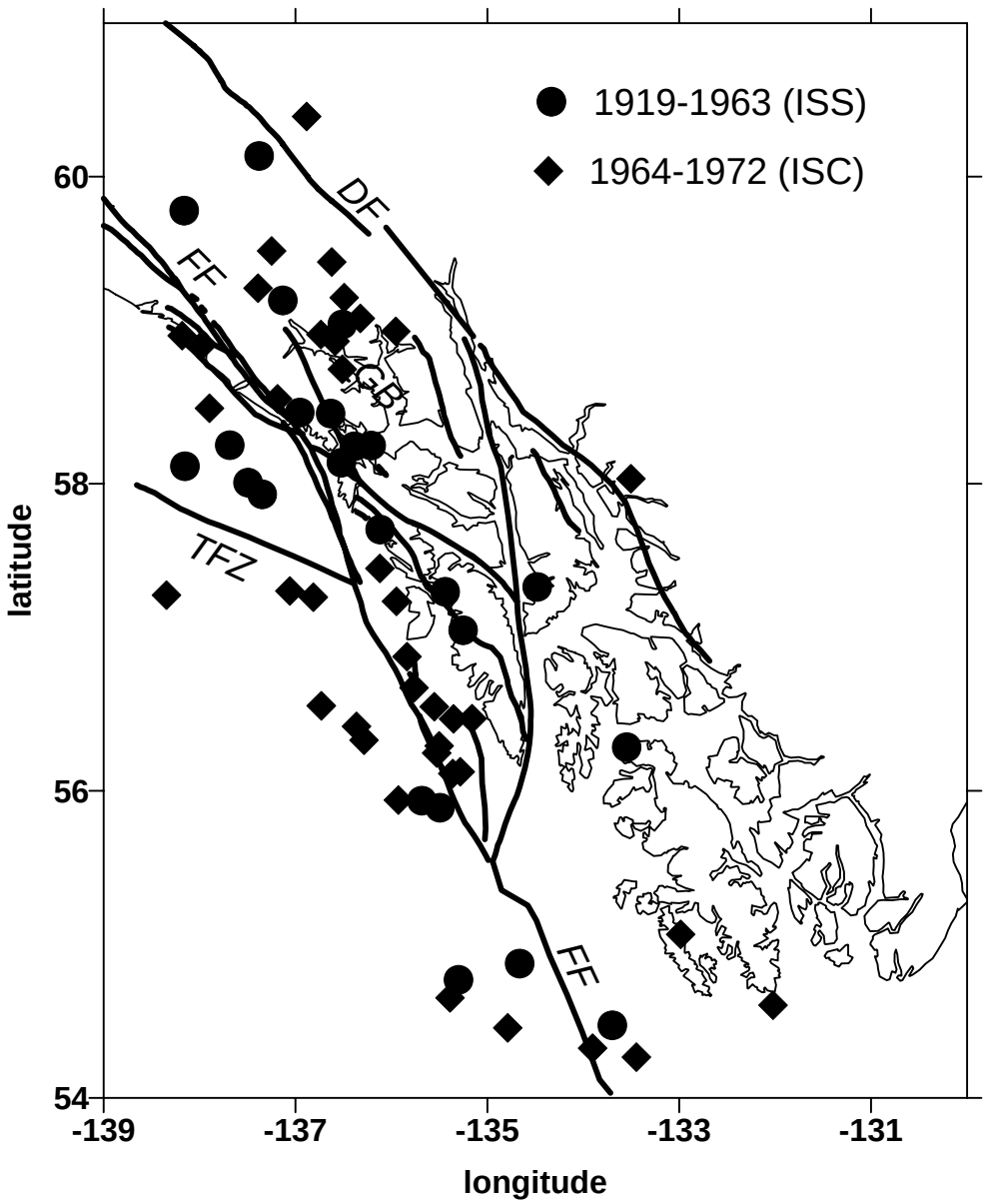

Figure 3 - Relocated earthquakes occurring prior to establishment of a local seismograph network. DF is Denali fault, FF is Fairweather fault, TFZ is Transition fault zone. GB is Glacier Bay

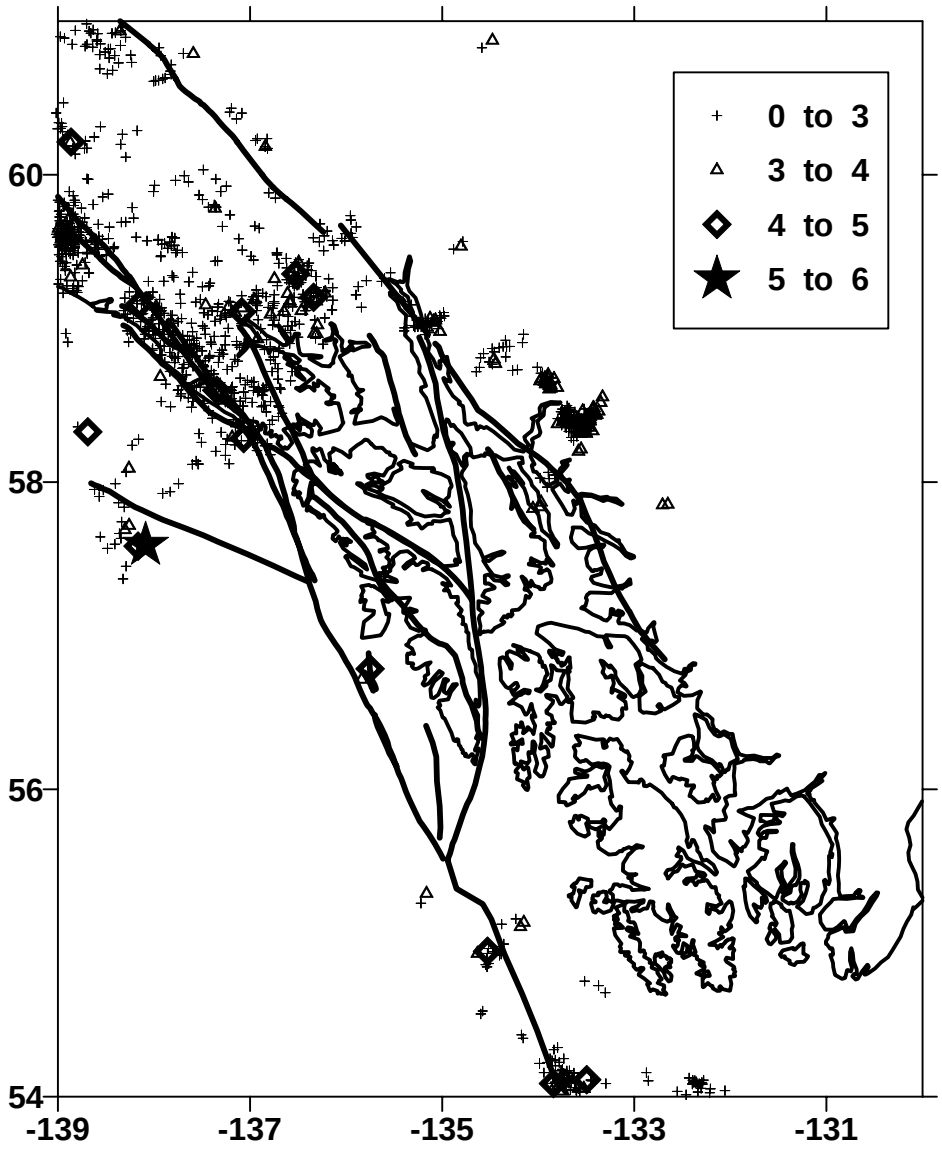

Figure 4 –Relocated earthquakes occurring between 1973 and 2005. Symbols are related to magnitude as indicated.

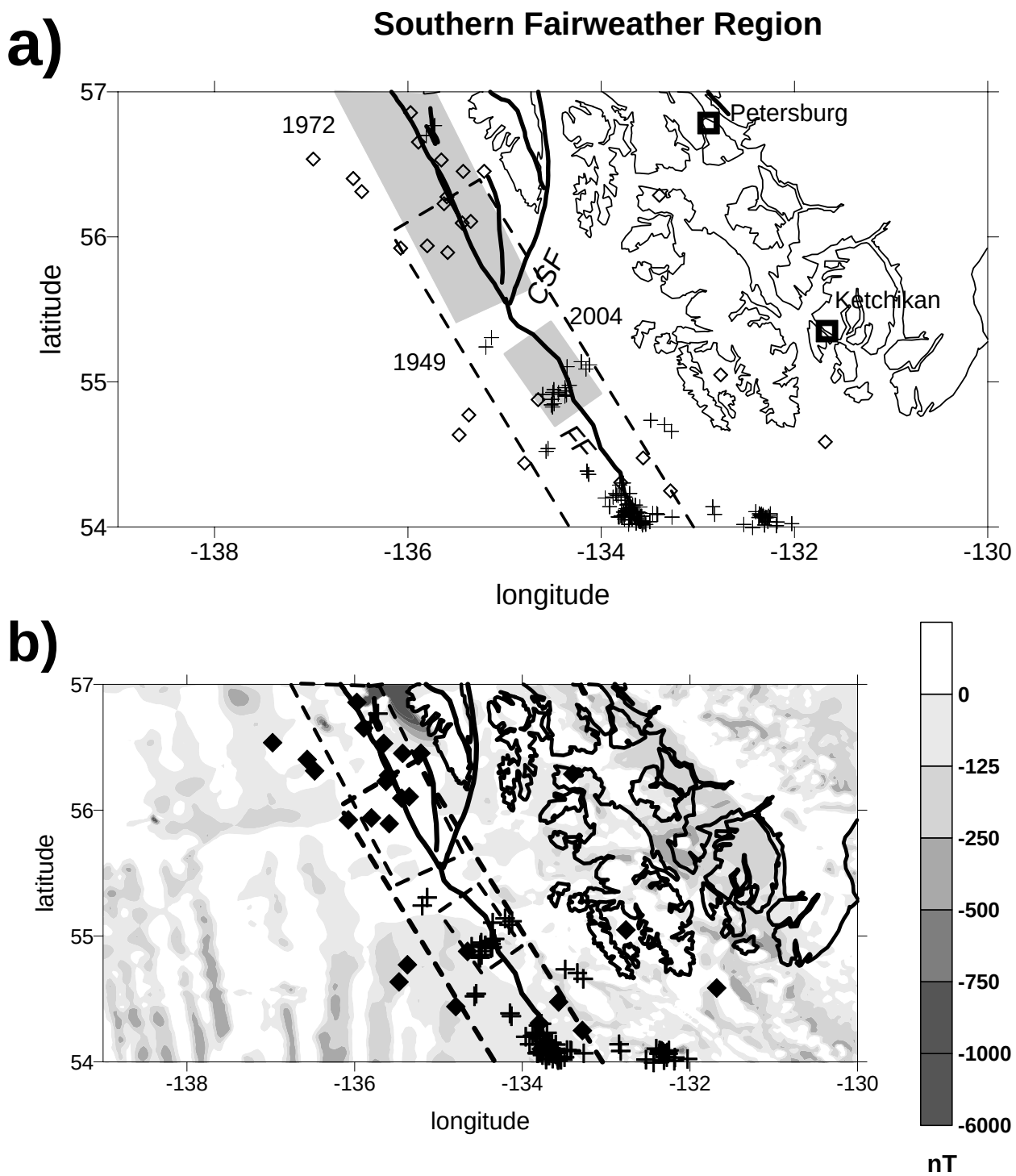

Figure 5 – Seismicity of southern Fairweather fault region. Plusses are earthquakes occurring between 1973 and 2005, diamonds are earthquakes occurring prior to 1973. (a) Seismicity compared to rupture along the Fairweather fault (gray boxes denote 1972 and 2004 ruptures, dashed lines denote 1949 rupture) in M>6.5 earthquakes. Squares are cities. CSF is Chatham Strait fault. FF is Fairweather fault (b) Seismicity compared to magnetic intensity (data from Saltus et al., 1999).

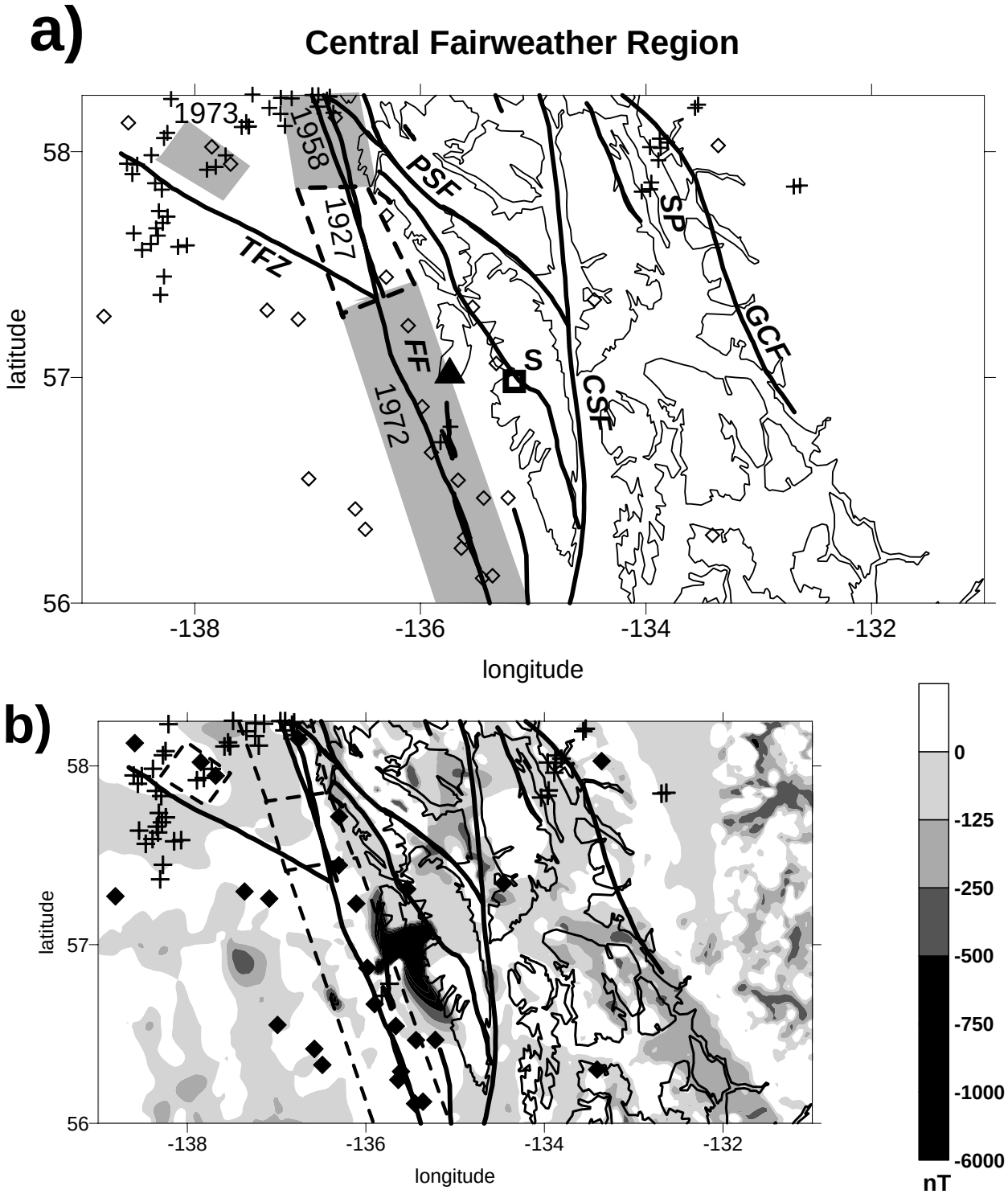

Figure 6 – Seismicity of the Central Fairweather region. (a) Gray boxes denote the 1972 and 1958 rupture zones along the Fairweather fault and rupture in the 1973 Cross Sound sequence (from Doser and Lomas, 2000). GCF is Gastineau Channel fault, PSF is Peril Strait fault, SP is Spencer Passage. Triangle is Mt. Edgecumbe volcano. Box labeled S is Sitka. (b) Magnetic intensity map based on data from Saltus et al. (1999). Large magnetic low is associated with Mt. Edgecumbe.

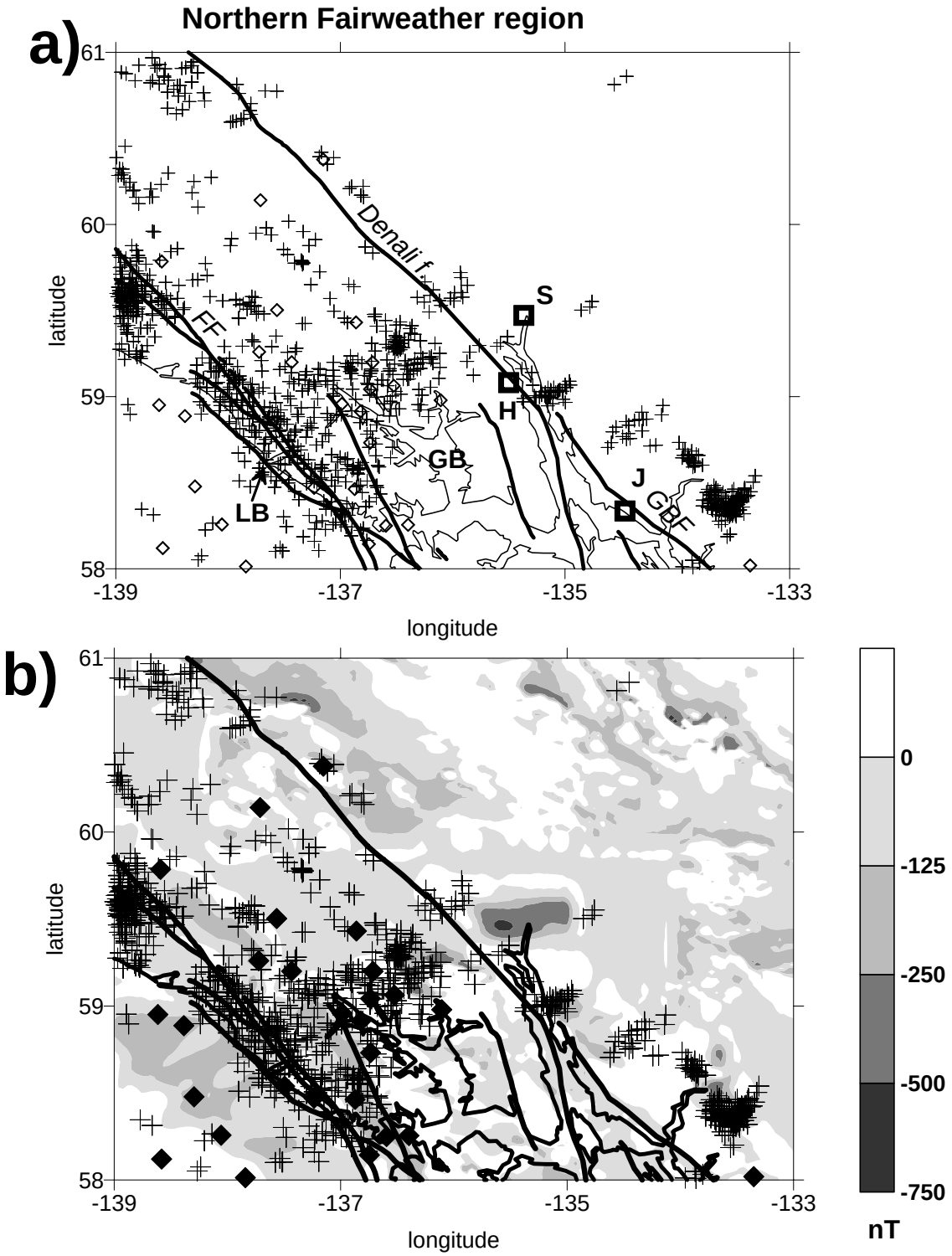
a)
Northern Fairweather region
Denali f.
FF
S
H
GB
J
GBF
LB
61
60
59
58
latitude
-139
-137
-135
-133
longitude
b)
0
-125
-250
-500
-750
nT

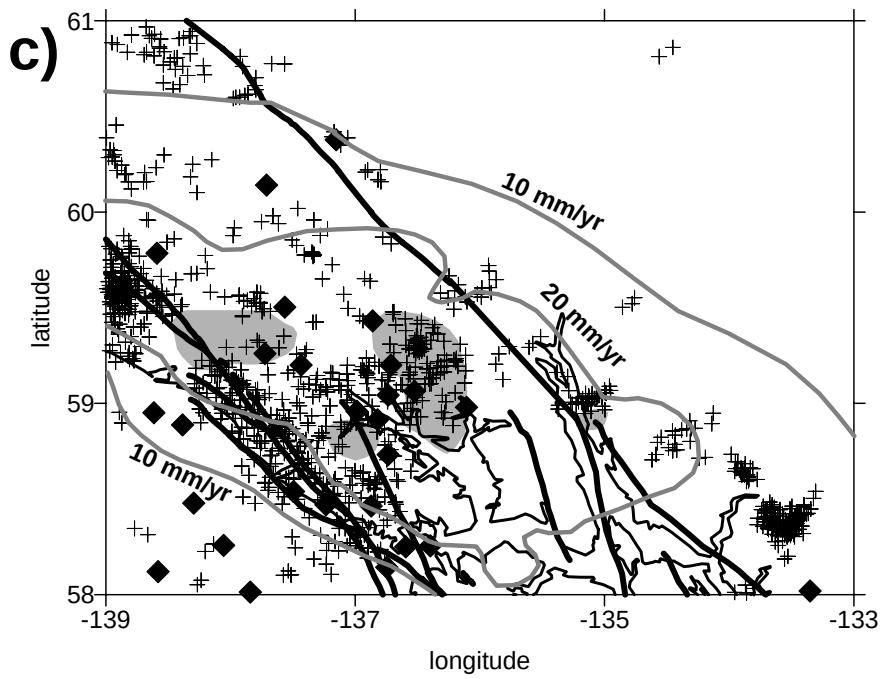

Figure 7- Seismicity of the northern Fairweather region. (a) Comparison to faults. Entire Fairweather fault (FF) shown in figure ruptured in 1958. S is Skagway, H is Haines, J is Juneau. LB is Lituya Bay and GB is Glacier Bay. GCF is Gastineau Channel fault. (b) Comparison to magnetic intensity data from Saltus et al. (1999). (c) Comparison to uplift data from Freymueller et al. (2008). Gray lines show contours of 10 and 20 mm/yr uplift. Gray shaded regions have uplift > 30 mm/yr.

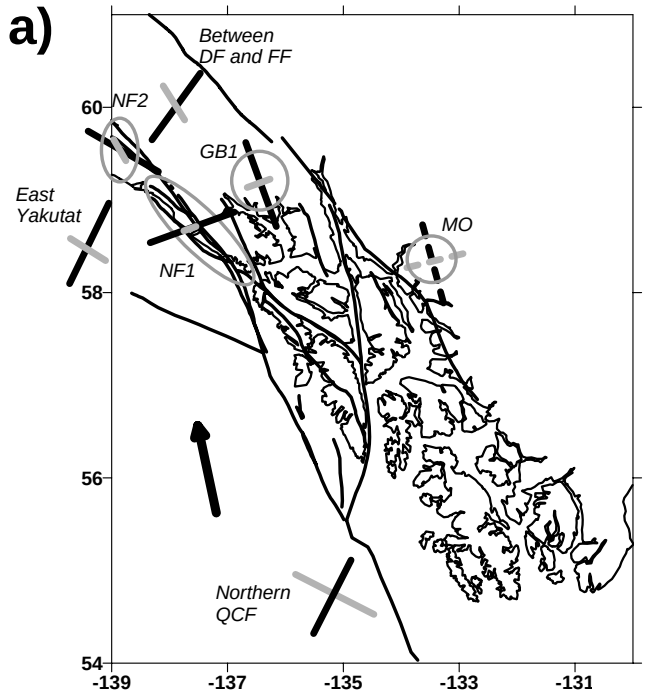

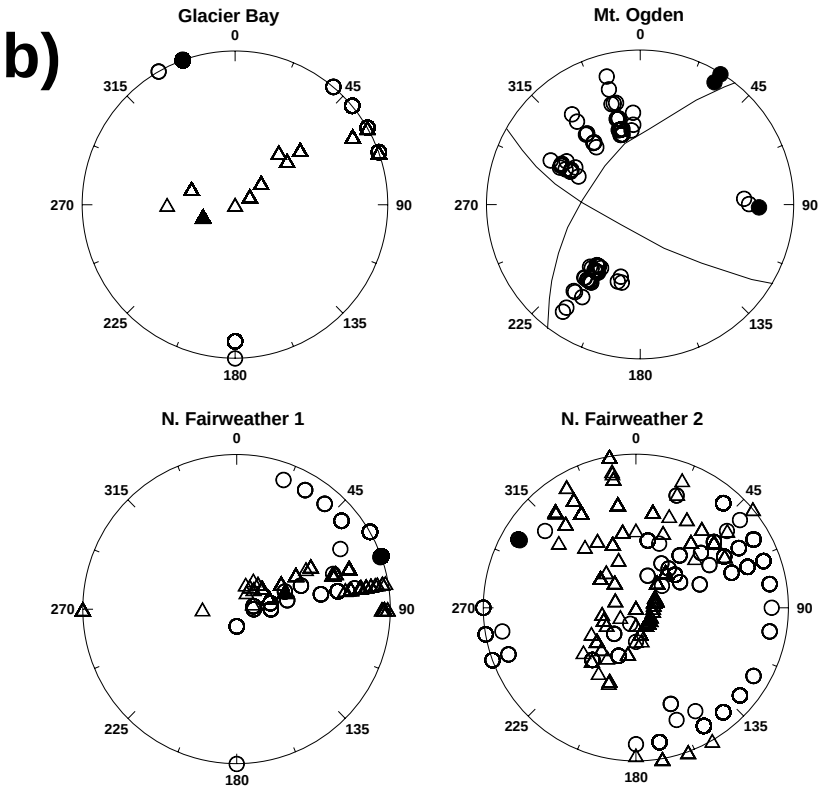

Figure 8 – Stress orientation information (a) Maximum (black) and minimum (gray) compressive stress directions (solid lines, see Table 1). Length of lines are proportional to plunge; the shorter the line, the higher the plunge angle. Ellipses indicate region used in stress inversions of this study. Dashed lines are P- and T-axes orientations. Arrow is direction of Pacific plate motion from DeMets and Dixon (1999). (b) Stress orientations from1000 repeated inversions of first motion data for Glacier Bay (GB), North Fairweather 1 (NF1) and North Fairweather 2 (NF2) regions shown in (a). Open triangles are minimum compressive stress directions and open circles are maximum compressive stress directions from iterations. Solid symbols are best fits to data. First motion data are shown for Mt. Ogden region along with the nodal planes that best fit the first motions and observed trend of regional seismicity.

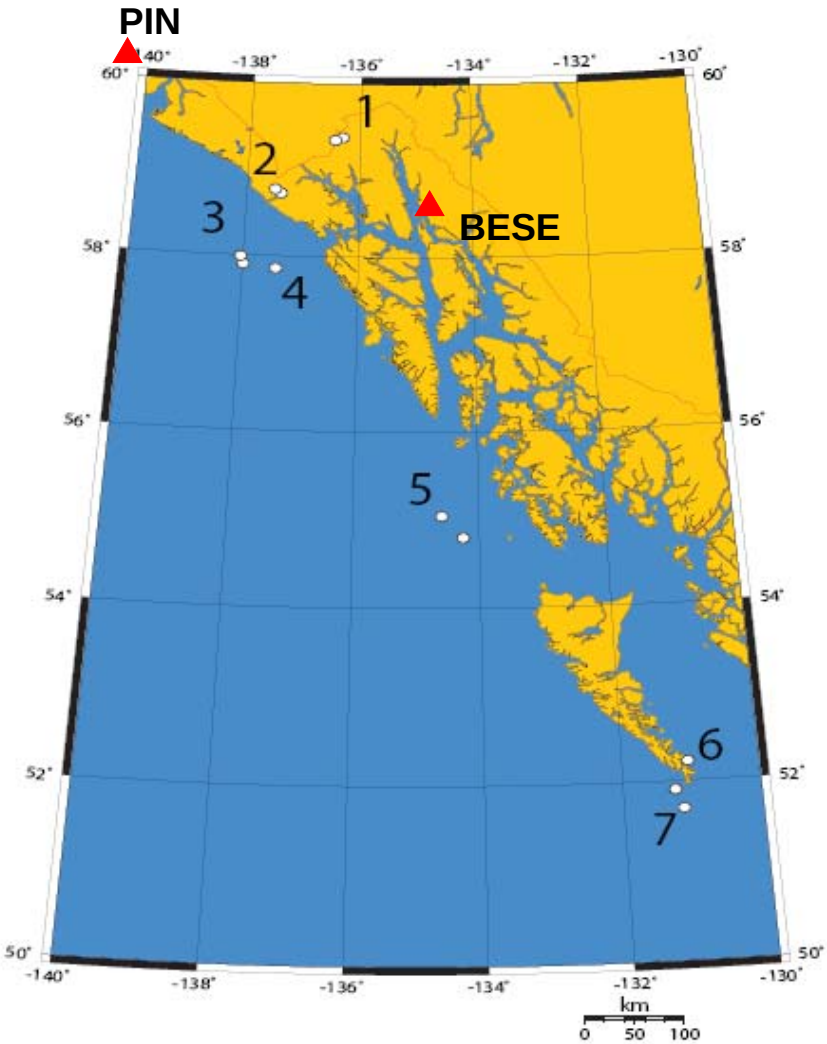

Figure 9 – Events used in empirical Greens function study. See Table 2 for details. Triangles labeled PIN and BESE are seismograph stations discussed in text.

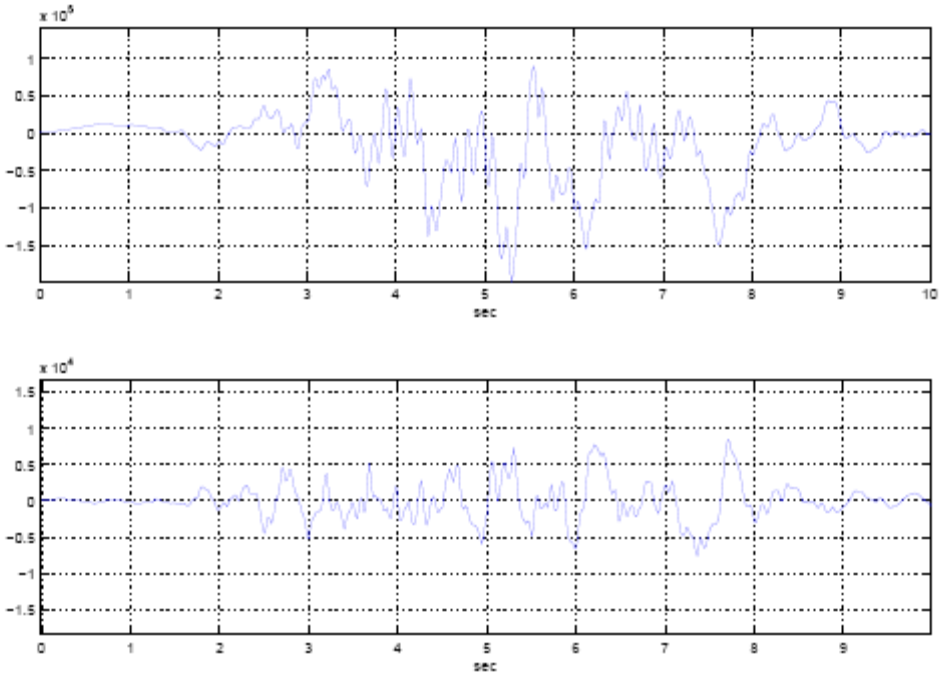

Figure 10 – Initial P-waveforms for the 6/28/2004 mainshock (top) and 7/4/2004 aftershock (bottom) recorded at station BESE (Figure 9).

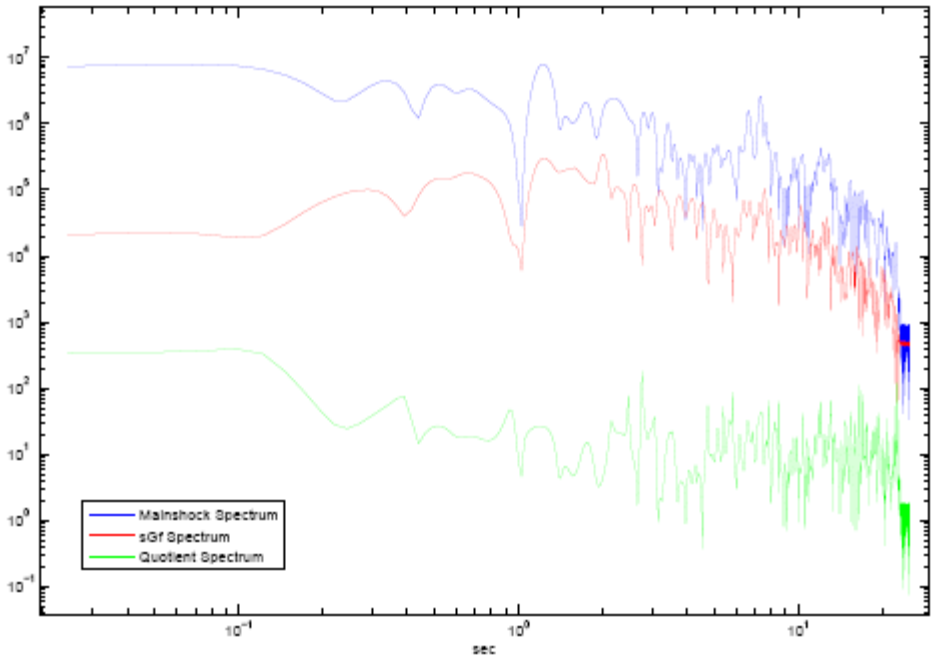

Figure 11 – Spectra of windowed P-arrivals for mainshock (blue) and aftershock (red) whose waveforms are shown in Figure 10. The quotient spectrum is shown in green.

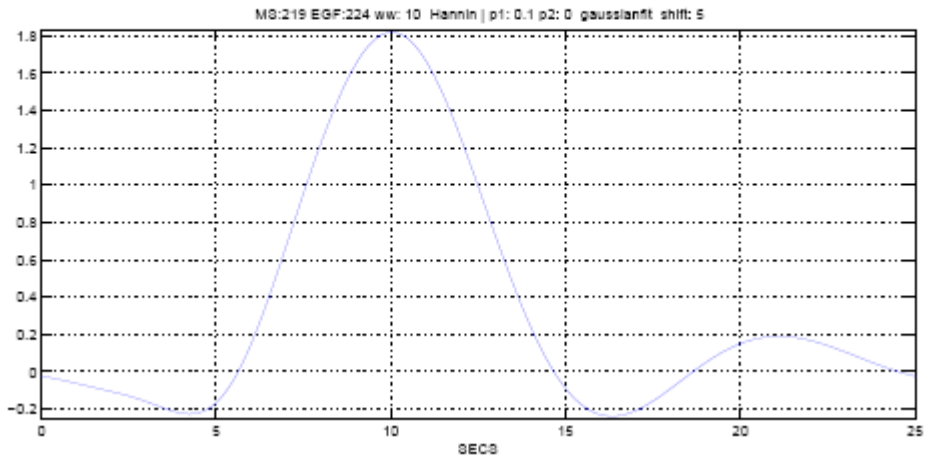

Figure 12 – Relative source time function of 6/28/2004 event scaled to the seismic moment of the 7/4/2004 aftershock (its empirical Greens function).

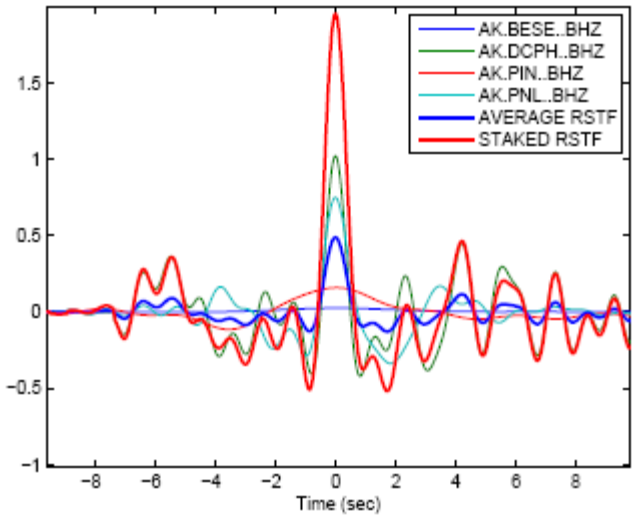

Figure 13 – Average (bold blue line) and stacked (bold red line) relative source time functions of the 8/4/2004 earthquake. Thinner lines represent single station estimates as indicated in the legend at upper right. Note that station PIN (Figure 9) shows the broadest pulse, suggesting rupture directed away from the station.

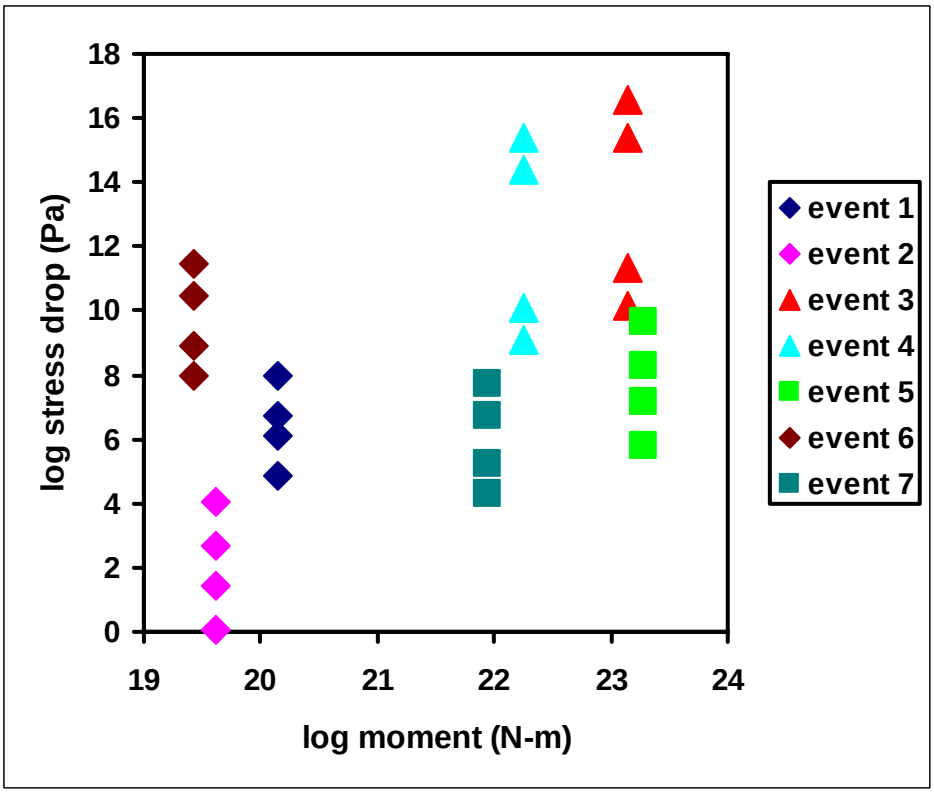

Figure 14 – Estimates of stress drop for events shown in Figure 9. Triangles are events of the 1973 Cross Sound sequence, squares are events on the Fairweather fault, and diamonds are events occurring off the fault (see Table 3 for details).

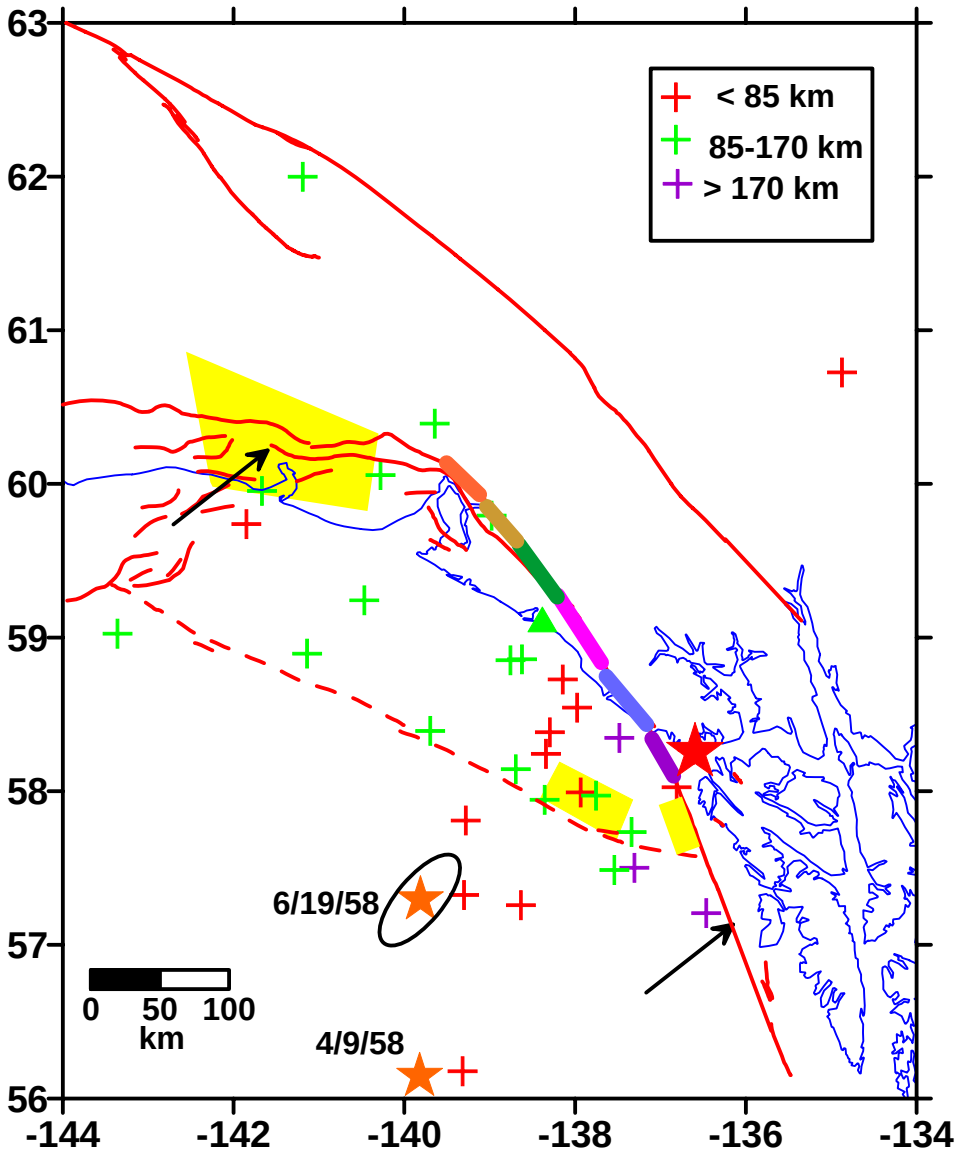

Figure 15 – Relocated aftershocks of the 1958 Fairweather earthquake (plusses) and two events (orange stars) occurring in the 3 months prior to the mainshock. Red star is mainshock location. Black arrows indicate probable extent of aftershock zone. Error ellipse for 6/19/58 event shows average orientation for relocations. The maximum lengths of the error ellipses for aftershocks are indicated by colors as noted in upper right. Yellow regions indicate the rupture zones of the 1979 St. Elias (northwest), 1973Cross Sound and 1927 Fairweather/Sitka earthquakes. Colored bold lines along Fairweather fault indicate possible position and length of subevents. Green triangle is mainshock intensity center from Doser (2009).

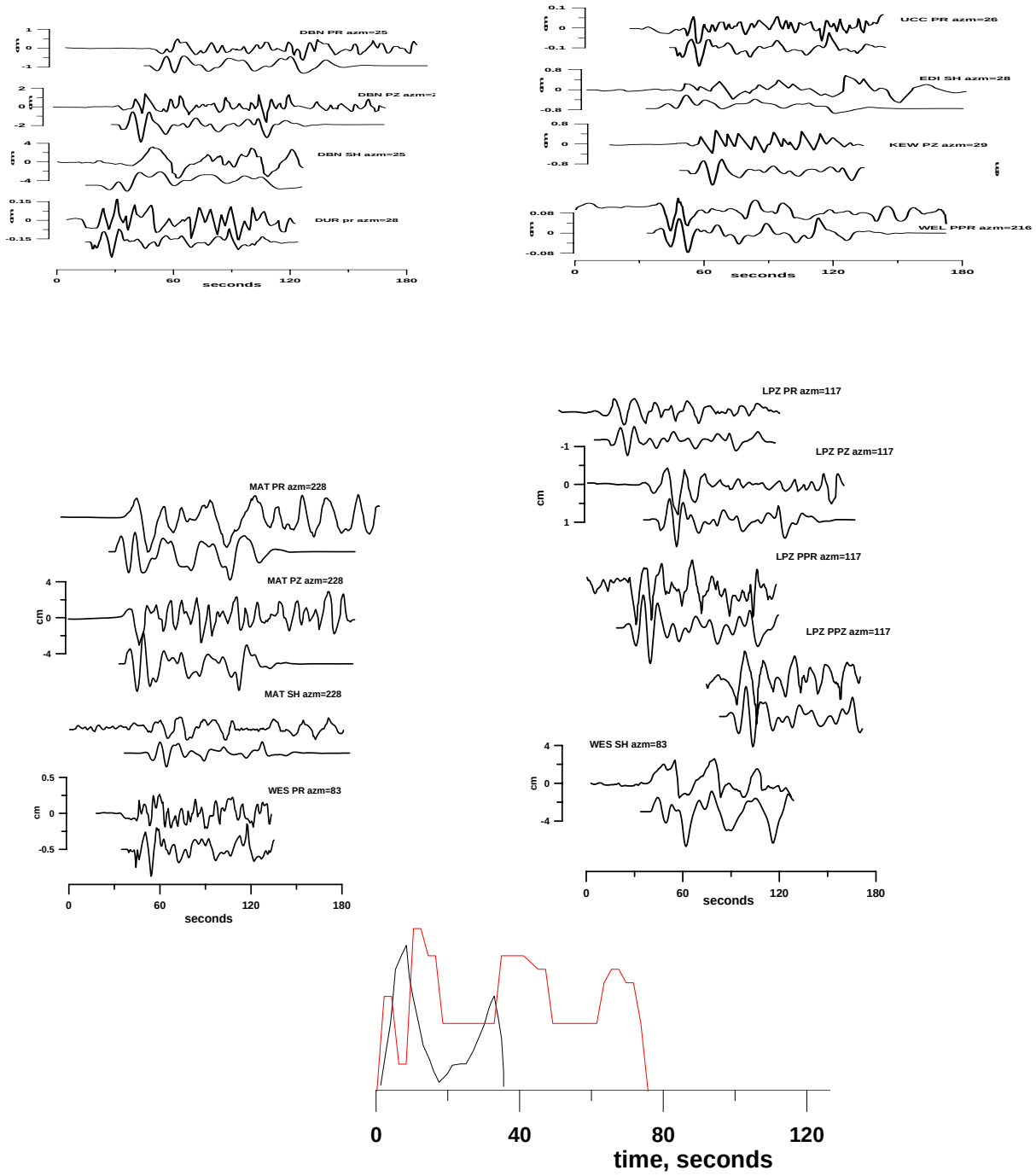

Figure 16 – Results of forward waveform modeling of the P-waves of the 1958 Fairweather seismograms. Top seismograms of each pair are observed, bottom are synthetic. S-waveforms are shown for reference but were not used in the forward modeling process. The new source time function is indicated by red lines at bottom. The old source time function from Doser and Loams (2000) is indicated by black lines.

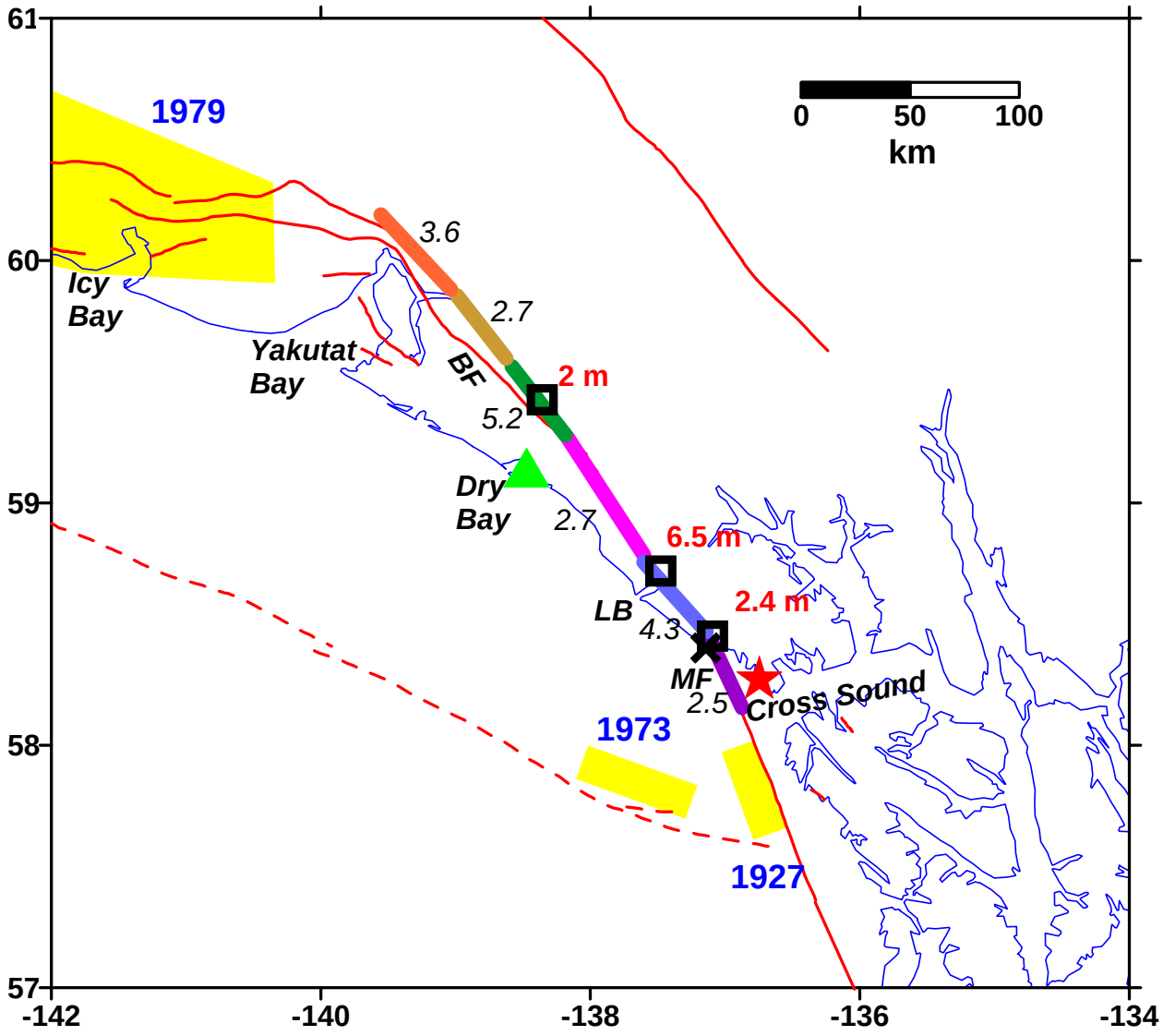

Figure 17 – Subevents of the 1958 Fairweather earthquake (bold colored lines) as estimated from the source time function shape (see Figure 16 and text). Squares represent points where Plafker et al. (1978) measured surface slip from the 1958 rupture (slip amount shown in red). Italic numbers indicate estimated seismic slip in meters along each fault segment. X labeled MF is Mt. Fairweather. LB is Lituya Bay. BF is Boundary fault. Yellow regions indicate rupture zones of other M>6.5 earthquakes. Red star is 1958 epicenter and green triangle is 1958 intensity center.

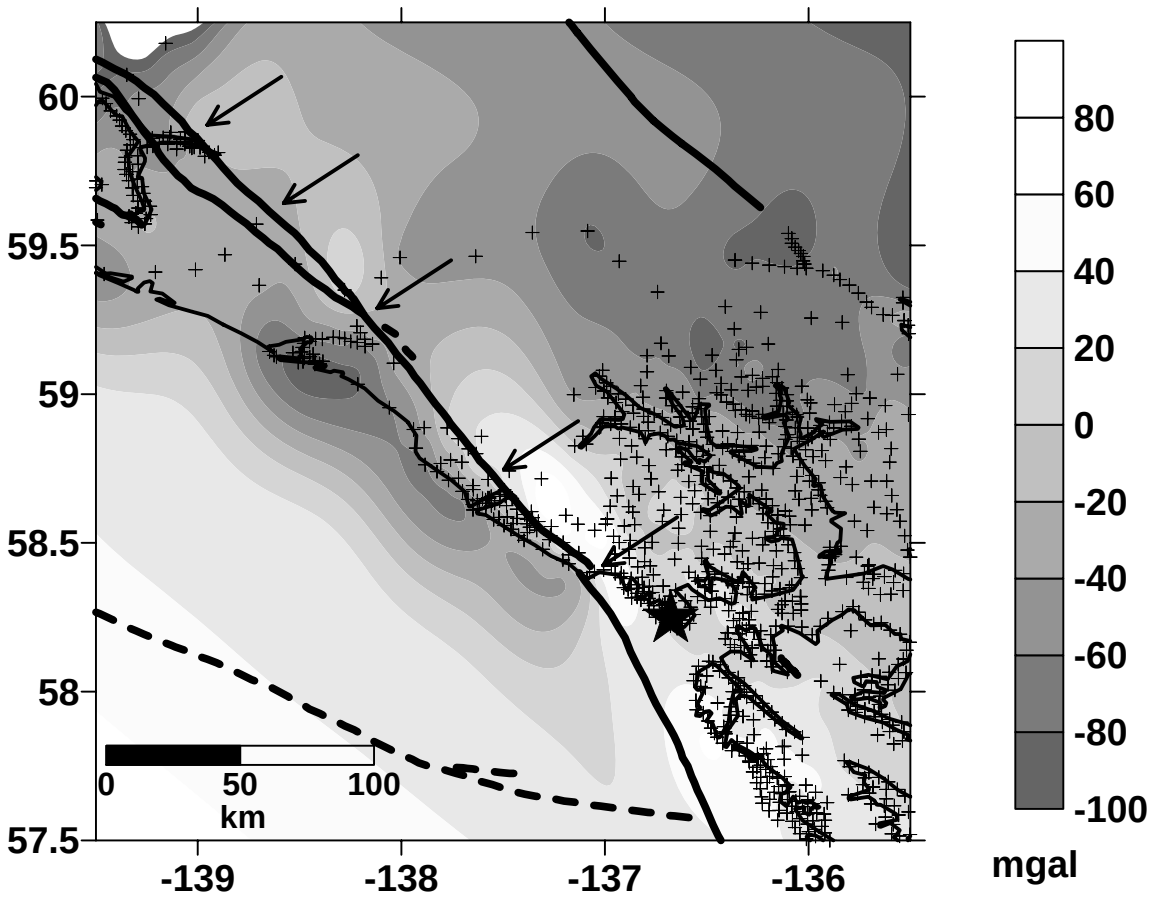

Figure 18 – Bouguer gravity anomaly map of northern Fairweather fault. The 1958 mainshock epicenter is indicated by star. Arrows indicate possible ends of subevent ruptures. Plusses indicate locations of gravity stations used to generate map.

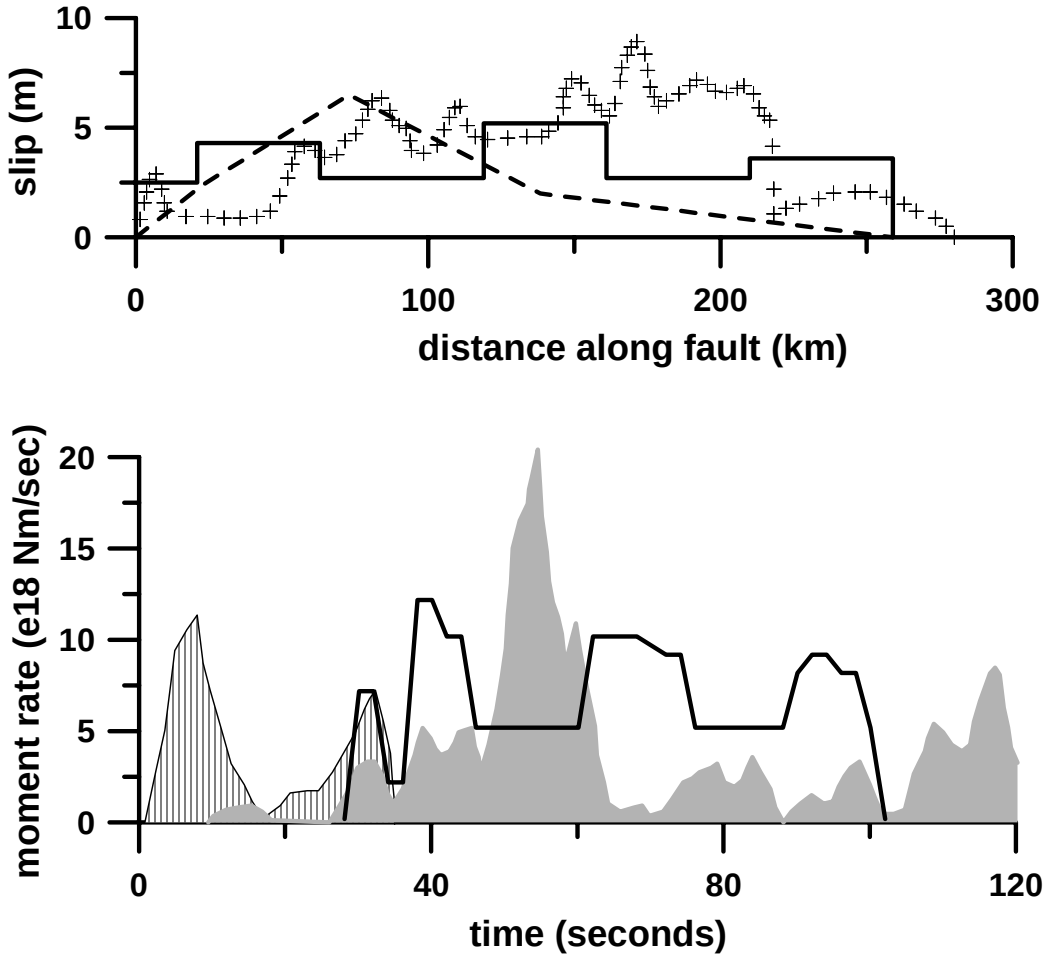

Figure 19 – Comparison of slip (top) and moment release (bottom) between the 1958 Fairweather and 2002 Denali fault earthquakes. Plusses are slip along Denali fault zone (Eberhart-Phillips et al., 2003). Dashed lines connect slip values measured by Plafker et al. (1978) along Fairweather fault. Solid line is slip estimated from source time function for 1958 event. Gray and striped filled regions indicate moment release estimated by Ozacar and Beck (2004) along the Denali fault and Susitna Glacier thrust, respectively. Bold line indicates moment release for 1958 Fairweather event.

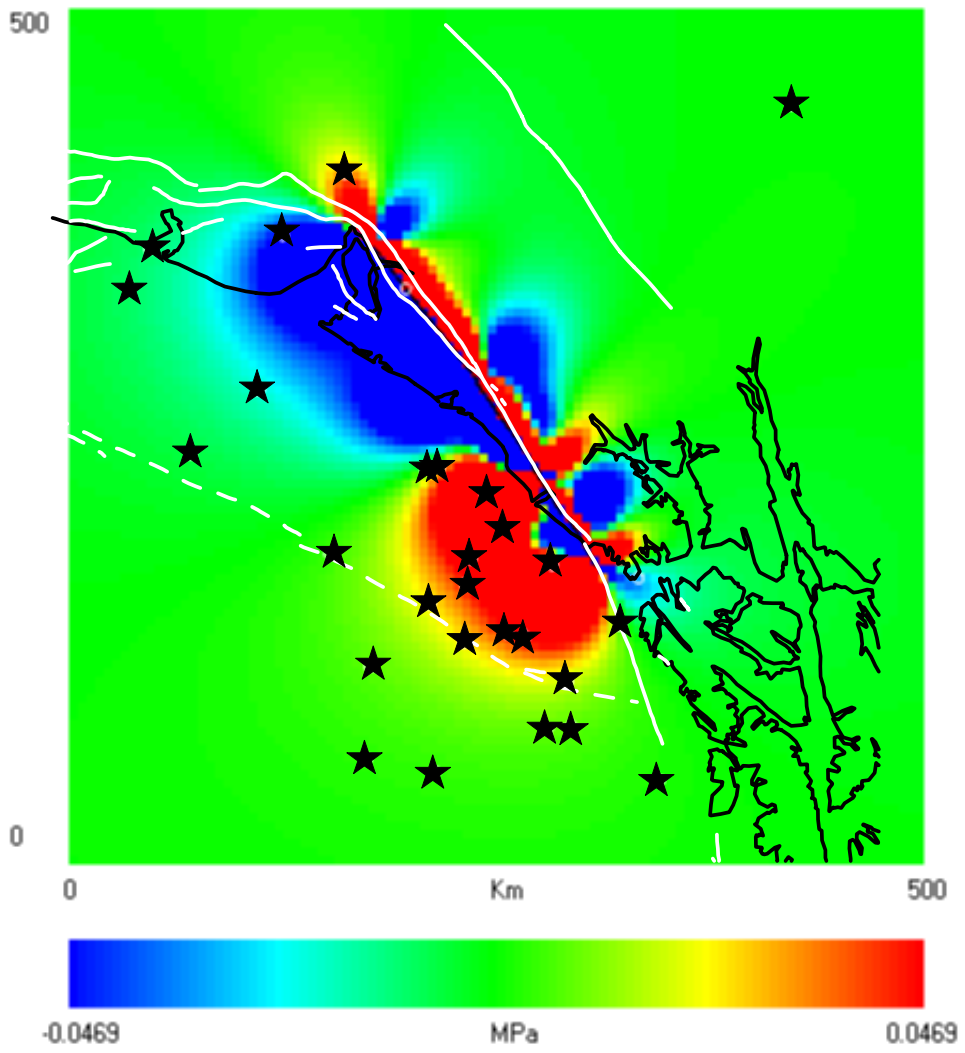

Figure 20 – Change in Coulomb failure stress (ΔCFS) following the 1958 mainshock on east-west oriented reverse faults (strike=260, dip=50, rake=110). Aftershock locations are indicated by stars.

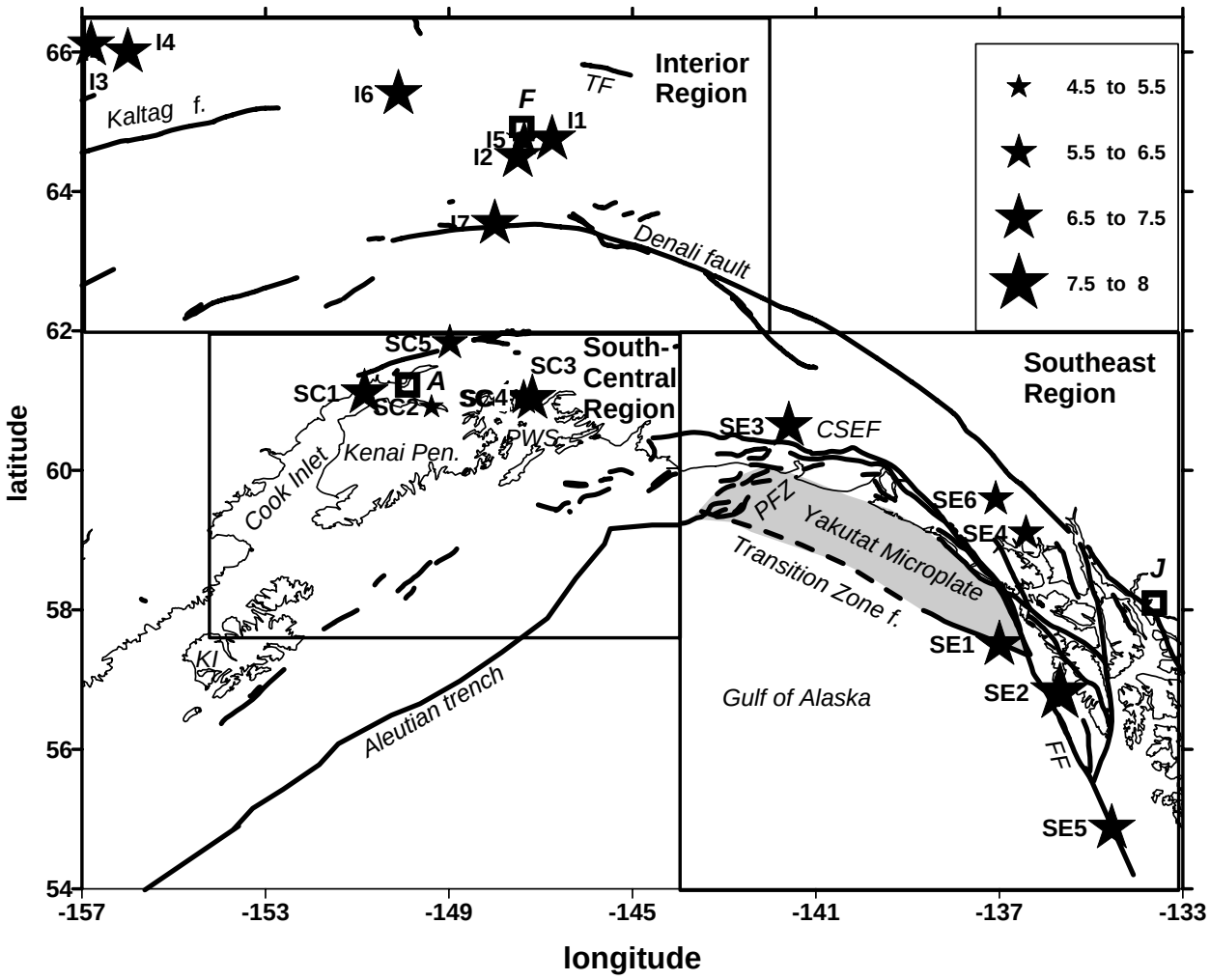

Figure 21 – Calibration events used to develop intensity-distance attenuation relationships for 3 regions of Alaska (Doser, 2009). Six calibration events were used to develop a relationship for Southeastern Alaska (SE1 to SE6). FF is Fairweather fault, PFZ is Pamplona fault zone, CSEF is Chugach-St. Elias fault. J is Juneau. The exposed portion of the Yakutat block is indicated by shading.

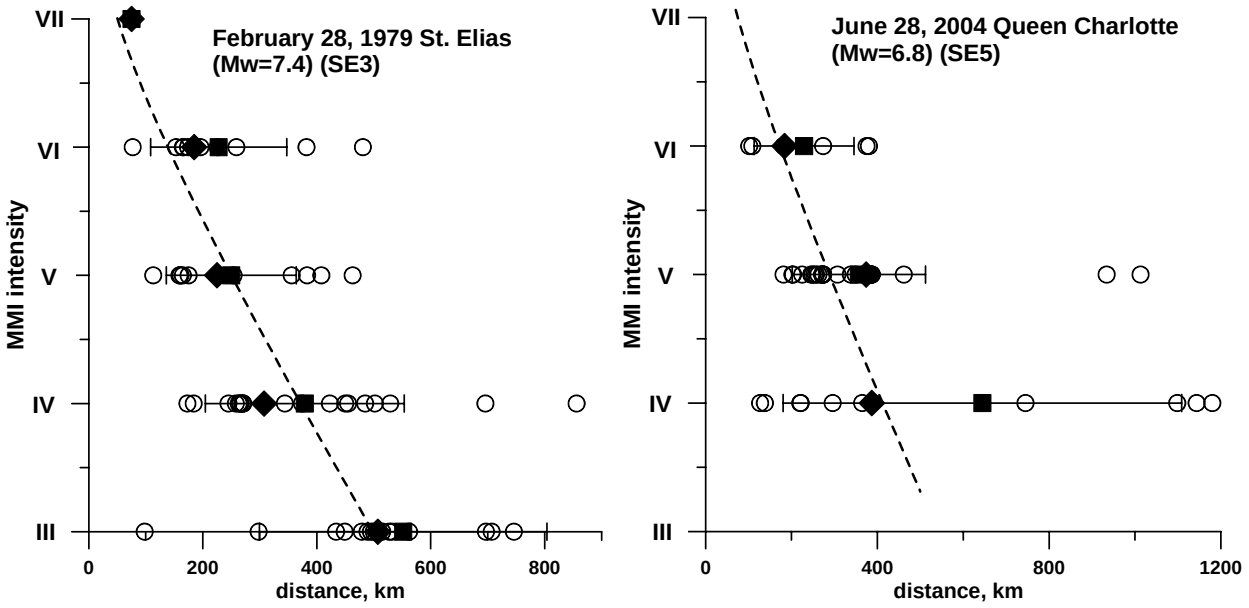

Figure 22 – MMI values versus hypocentral distance for two southeast Alaska calibration events (see Figure 21 for locations). Circles represent individual observed intensity values. Mean and median epicentral distance for each intensity-source pair are denoted by the solid squares and diamonds, respectively. Error bars represent ± one standard deviation of the data. The dashed lines denote the predicted MMI versus distance model for southeast Alaska.

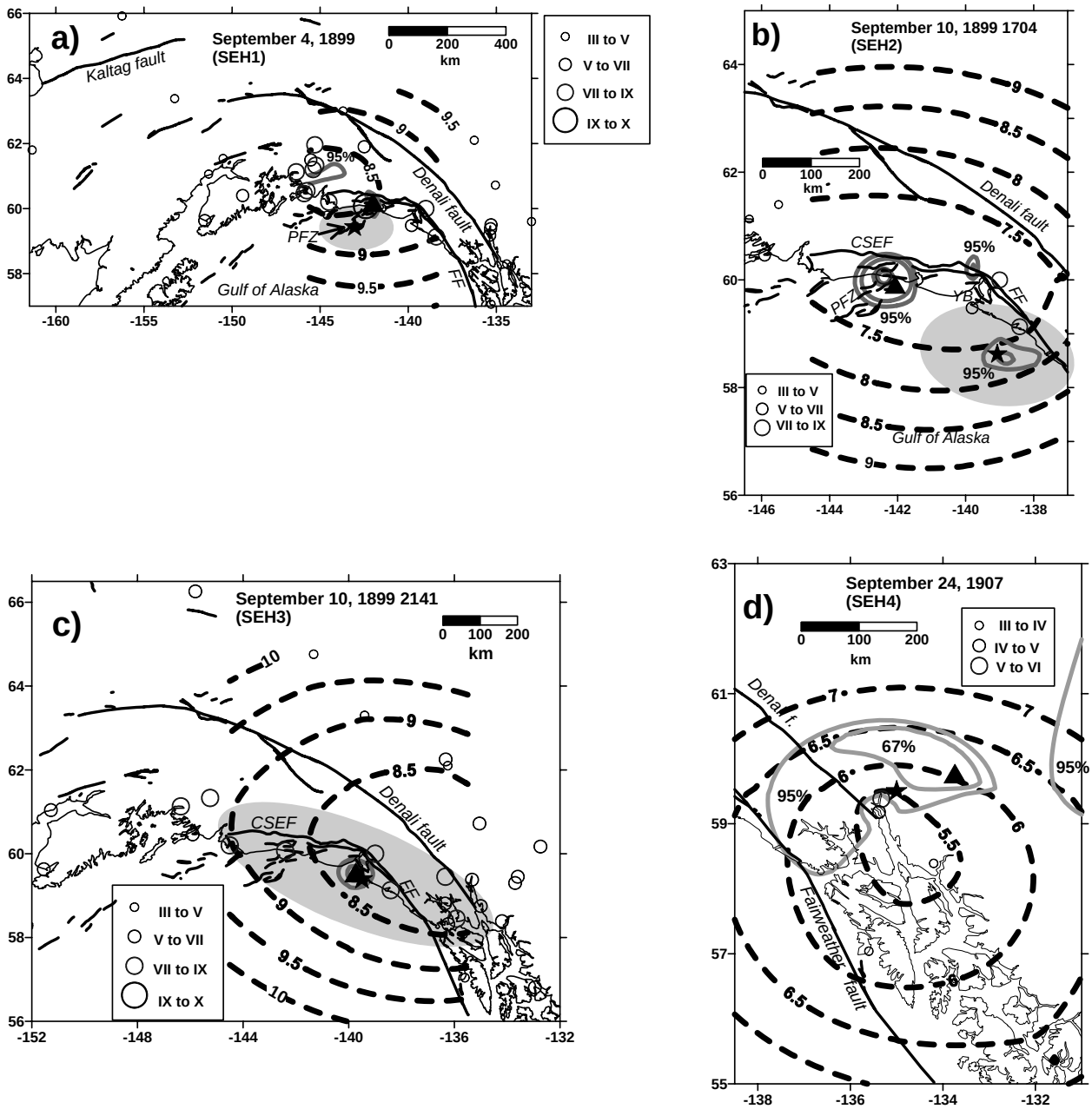
a)
September 4, 1899
(SEH1)
0 200 400
km
III to V
V to VII
VII to IX
IX to X
Kaltag fault
Denali fault
PFZ
FF
Gulf of Alaska
95%
9
9.5
8.5
b)
September 10, 1899 1704
(SEH2)
0 100 200
km
CSEF
PFZ
YB
FF
Denali fault
Gulf of Alaska
95%
9
8.5
8
7.5
III to V
V to VII
VII to IX
c)
September 10, 1899 2141
(SEH3)
0 100 200
km
CSEF
Denali fault
FF
III to V
V to VII
VII to IX
IX to X
10
9
9.5
8.5
d)
September 24, 1907
(SEH4)
0 100 200
km
III to IV
IV to V
V to VI
Denali f.
Fairweather fault
67%
95%
7
6.5
6
5.5

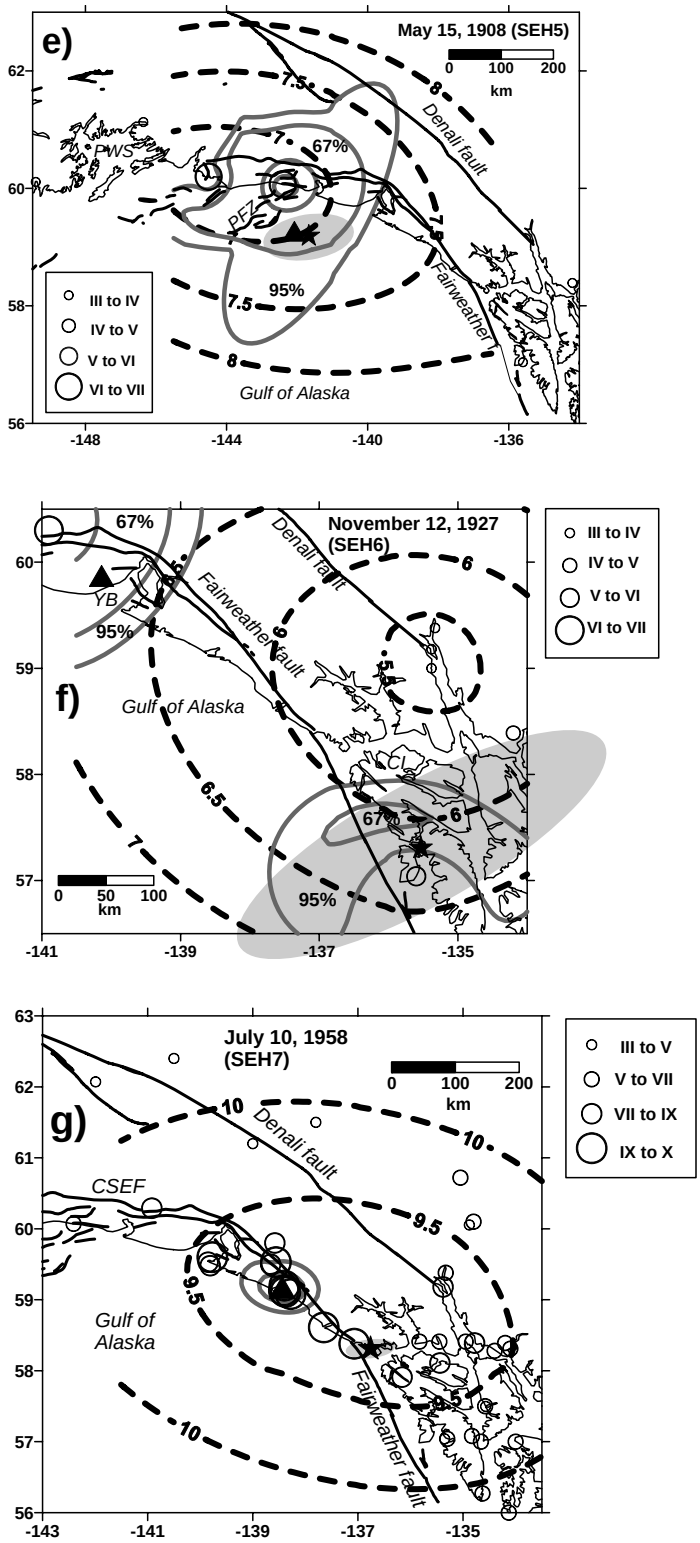

Figure 23 - Plots of intensity observations (open circles), instrumental location (gray error ellipses), intensity location (gray lines), and estimates of M_{MMI} (intensity magnitude, bold dashed lines) for historic events of the southeast Alaska region The gray lines represent the 95% (outer) and 67% (inner) location confidence contours. Intensity center is indicated by triangle,

epicenter by star. (a) September 4, 1899 Yakutat earthquake, FF is Fairweather fault, PFZ is Pamplona fault zone (b) September 10, 1899 (1704 UTC) Yakutat earthquake, CSEF is Chugach-St. Elias fault zone, (c) September 10, 1899 (2141 UTC) Yakutat earthquake, (d) September 24, 1907 southern Denali fault earthquake, (e) May 15, 1908 Yakutat earthquake, PWS is Prince William Sound, (f) November 12, 1927 Sitka aftershock, CI is Chicagof Island, YB is Yakutat Bay, (g) July 10, 1958 Fairweather earthquake. Intensity observations for the 1958 Fairweather event from southern British Columbia and far western Alaska are not shown.